

Technical report 09-050

Distributed Predictive Control for Energy Hub Coordination in Coupled Electricity and Gas Networks*

M. Arnold, R. R. Negenborn, G. Andersson, and B. De Schutter

To cite this work, please refer to the published version:

M. Arnold, R. R. Negenborn, G. Andersson, and B. De Schutter, “Distributed predictive control for energy hub coordination in coupled electricity and gas networks,” Chapter 10 in *Intelligent Infrastructures* (R. R. Negenborn, Z. Lukszo, and H. Hellendoorn, eds.), vol. 42 of *Intelligent Systems, Control and Automation: Science and Engineering*, Dordrecht, The Netherlands: Springer, ISBN 978-90-481-3598-1, pp. 235–273, 2010. doi:[10.1007/978-90-481-3598-1_10](https://doi.org/10.1007/978-90-481-3598-1_10)

Delft Center for Systems and Control
Delft University of Technology
Mekelweg 2, 2628 CD Delft
The Netherlands
phone: +31-15-278.24.73 (secretary)
URL: <https://www.dcsc.tudelft.nl>

* This report can also be downloaded via <https://dpub.eu/09-050>

Chapter 1

Distributed Predictive Control for Energy Hub Coordination in Coupled Electricity and Gas Networks

M. Arnold, R.R. Negenborn, G. Andersson, and B. De Schutter

Abstract In this chapter, the operation and optimization of integrated electricity and natural gas systems is investigated. The couplings between these different infrastructures are modeled by the use of energy hubs. These serve as interface between the energy consumers on the one hand and the energy sources and transmission lines on the other hand. In previous work, we have applied a distributed control scheme to a static three-hub benchmark system, which did not involve any dynamics. In this chapter, we propose a scheme for distributed control of energy hubs that do include dynamics. The considered dynamics are caused by storage devices present in the multi-carrier system. For optimally incorporating these storage devices in the operation of the infrastructure, their capacity constraints and dynamics have to be taken into account explicitly. Therefore, we propose a distributed Model Predictive Control (MPC) scheme for improving the operation of the multi-carrier system by taking into account predicted behavior and operational constraints. Simulations in which the proposed scheme is applied to the three-hub benchmark system illustrate the potential of the approach.

M. Arnold, G. Andersson
ETH Zürich, Power Systems Laboratory, Zürich, Switzerland,
e-mail: arnold,andersson@eeh.ee.ethz.ch

R.R. Negenborn
Delft University of Technology, Delft Center for Systems and Control, Delft, The Netherlands,
e-mail: r.r.negenborn@tudelft.nl

B. De Schutter
Delft University of Technology, Delft Center for Systems and Control & Marine and Transport
Technology, Delft, The Netherlands, e-mail: b@deschutter.info

1.1 Introduction

1.1.1 Multi-carrier systems

Most of today's energy infrastructures evolved during the second part of the last century and it is questionable whether these infrastructures will meet tomorrow's requirements on flexibility and reliability if their operation is not made more intelligent. The on-going liberalization of the energy markets involves extended cross-border electricity trading and exchange activities, which implicate that electricity networks have to operate closer and closer to their capacity limits. In addition, issues such as the continuously growing energy demand, the dependency on limited fossil energy resources, the restructuring of power industries, and the increasing societal desire to utilize more sustainable and environmentally friendly energy sources represent future challenges for both energy system planning and operation.

Nowadays, different types of infrastructures, such as electricity, natural gas, and local district heating infrastructures, are mostly planned and operated independently of each another. However, the integration of distributed generation plants, such as so-called co-generation and tri-generation plants [7, 13] links these different types of infrastructures. E.g., small-scale combined heat and power plants (μ CHP) consume natural gas to produce electricity and heat simultaneously. In this way, such systems affect infrastructures for electricity and gas networks, as well as infrastructures for district heating. As the number of such generation units increases, the different infrastructures become more and more coupled.

Several conceptual approaches have been examined for describing systems including various forms of energy. Besides "energy-services supply systems" [11], "basic units" [5], and "micro grids" [18], so-called "hybrid energy hubs" [10] are proposed to address these kind of systems. The latter formulation has been established within the project "Vision of Future Energy Networks", which has been initiated at ETH Zürich. In this project, a general modeling and optimization framework is developed for multi-carrier energy systems, so-called "hybrid energy systems", where the term "hybrid" indicates the usage of multiple energy carriers. The couplings between the different energy carriers are taken into account by the energy hub concept, with which storage of different forms of energy and conversion between them is described. Principally, energy hubs serve as interface between the consumers and the transmission infrastructures of the different types of energy systems.

Because of the increasing number of distributed generation facilities with mostly intermittent energy infeed (generation profiles), the issue of storing energy becomes more important. Electric energy storage devices are expensive and their operation causes energy losses. A more effective option is the operation of a μ CHP device in combination with a heat storage device. By means of the heat storage device, the μ CHP device can be operated with a focus on following the electric load while storing the simultaneously produced heat. In general, the trend does not go towards large storages but rather in direction of small local storages, such as local hot water

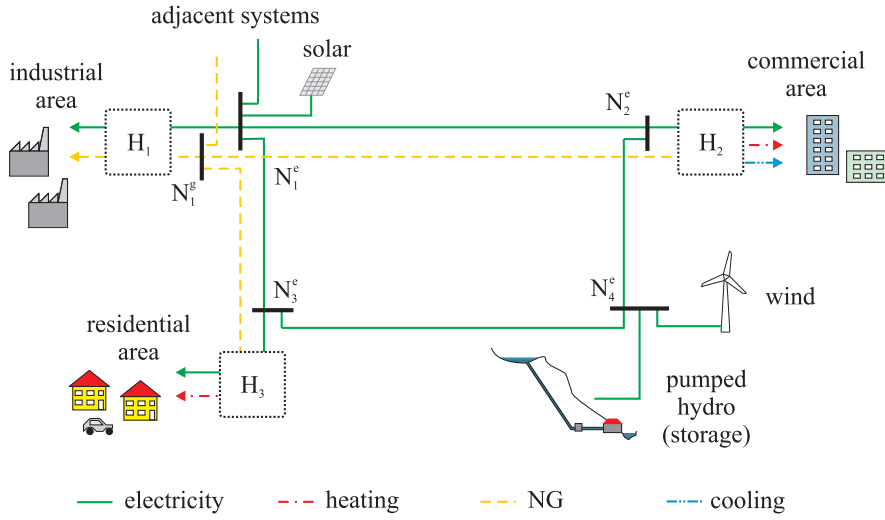


Fig. 1.1: Sketch of a system of three interconnected energy hubs.

storages within households. Beyond that, it could be expected that within the next 20 years, a huge amount of small and cheap energy storage units will be available, provided by PHEVs (plug-in hybrid electric vehicles).

Recently, research has addressed the *integrated* control of combined electricity and natural gas systems, e.g., in [2, 3, 21, 26]. While [21, 26] analyze the impact of natural gas infrastructures on the operation of electric power systems, [2, 3] directly address the integrated natural gas and electricity optimal power flow.

Figure 1.1 illustrates an exemplary hub based energy system supplied and interconnected by natural gas and electricity networks. The electricity network comprises four network nodes (N₁^e–N₄^e), whereas the natural gas network only features one network node N₁^g. Three hubs are present in the system, where each hub interfaces the natural gas and electricity distribution networks with the corresponding supply area. This illustration represents the supply of a town that is divided into industrial (hub H₁), commercial (hub H₂), and private/residential load (hub H₃) supply areas. The internal structure of each hub depends on the specific loads present at that hub. For example, hubs may contain electrical transformers, gas turbines, furnaces, heat exchangers, etc., but also storage devices such as heat storages or batteries. In the depicted system, both natural gas and electricity is exchanged with adjacent systems via network nodes N₁^g and N₁^e. Furthermore, a solar power plant is connected to the electric network node N₁^e as a power generation source outside the hub. Besides that, N₄^e connects the system with hydro and wind power plants.

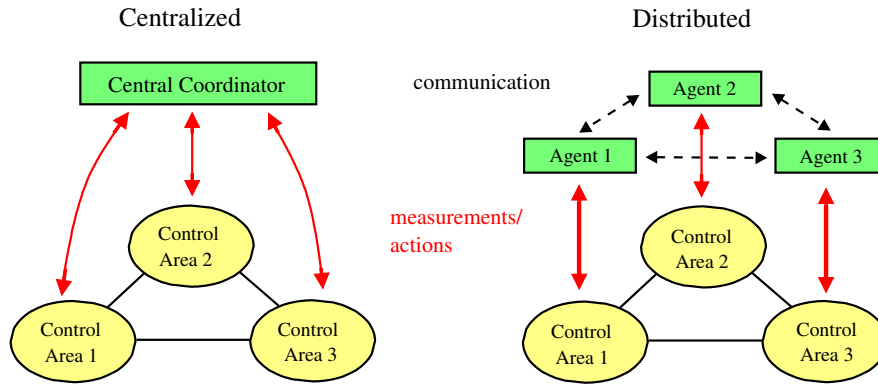


Fig. 1.2: Sketch of a centralized and distributed control architecture for a system of three interconnected control areas. The solid arrows refer to measurements/actions between the physical system and the control unit(s). Information exchange between control units is indicated by dashed arrows.

1.1.2 Control of energy hubs

To determine the optimal operation of a multi-carrier energy system, an optimal power flow problem has to be solved. An optimal power flow problem is a general optimization problem, which is formulated as an objective to be minimized, subject to system constraints to be satisfied. In particular, the power flow equations of the different energy carriers are part of these system constraints. By solving this optimal power flow problem, the optimal operational set-points of the system, i.e., of the energy generation units, converters and storage devices, can be determined.

In the considered model storage devices with dynamic behavior are present. Since these storage devices cause a dependency between consecutive time steps, optimization over multiple time steps is required. Therefore, for the optimal operation of the system, actions have to be determined taking the expected future behavior of the system into account. For optimizing the operation over multiple time steps, we propose to use model predictive control (MPC) [6, 19]. MPC is widely used in different application areas, since system dynamics, data forecasts, and operational constraints (system constraints) can be taken into account explicitly. In our case, we use MPC to determine the actions for the individual energy hubs that give the best predicted behavior, e.g., minimal energy costs, based on characteristics of the transmission infrastructures, the dynamics of the storage devices, and the load and price profiles. By using this predictive approach, the energy usage can be adapted to expected fluctuations in the energy prices, as well as to expected changes in the load profiles.

In an ideal situation, a centralized, supervisory controller can measure all variables in the network and determines actions for all actuators. This centralized controller solves at each decision step one optimization problem to determine actions

for the entire system. The centralized control architecture is shown on the left-hand side in Figure 1.2, where a central coordinator supervises three interconnected control areas, e.g., hubs. Although for small-scale systems, centralized control may work well, for large-scale systems, a high amount of data needs to be transferred along the whole system and large optimization problems will have to be solved, resulting in high computational requirements. In addition, for large-scale systems, it may simply not be possible to have a single controller controlling all areas, in the case that these areas are owned by different parties. These difficulties could be overcome by implementing a distributed approach as explained in the following.

When solving the optimization problem in a distributed manner, each control area is controlled by its own respective control authority. Applying distributed control, the overall optimization problem is divided into subproblems which are solved in an iterative procedure. In order to guarantee the energy supply of the entire system, the control authorities have to coordinate their actions among one another (Figure 1.2, right-hand side).

The differences between centralized and distributed control in terms of supervision, synchronization, and type of optimization problem are summarized in Table 1.1. Distributed control has several advantages over centralized control. Distributed control is better suited for a distributed power generation infrastructure like the one considered in this chapter, since in distributed control the sometimes conflicting objectives of the individual hubs can explicitly be taken into account. Furthermore, distributed control has the potential to achieve higher robustness, since if the agent of one area fails, only this specific area is not controlled anymore, while other areas are still controlled. Furthermore, shorter computation times arise in distributed control, particularly for larger-scale systems. The control problems of the individual controllers are smaller in size and these local control problems can often be solved in parallel. The challenge is to design efficient coordination and communication among the individual controllers that provides overall system performance comparable to a centralized control authority.

Several approaches have been proposed for distributed control over the last decades, enabling coordination within a multi-area system. In [25] a variety of distributed MPC approaches applied to different application areas is summarized. The

Table 1.1: Centralized versus distributed control.

	Centralized	Distributed
Supervision	Central coordinator supervises all areas	Each area is supervised by its agent only
Synchronization	Areas send data to a central coordinator	Agents exchange data among each other
Optimization problem	Central coordinator performs overall optimization problem	Overall optimization problem is decomposed into subproblems

main approaches adopted are reviewed and a classification of a number of decentralized, distributed, and hierarchical control architectures for large-scale systems is proposed. Particular attention is paid to design approaches based on MPC. In [1] a decentralized MPC approach for linear, time-invariant discrete systems where the subproblems are solved in a noniterative way is proposed. In [22] a distributed MPC scheme based on decompositions of augmented Lagrangians is proposed for control of interconnected linear systems. In [28] a distributed MPC algorithm is presented where each local controller tends to move towards a Nash equilibrium by means of game theory considerations. This algorithm is based on discrete linear time invariant systems, too.

Work on distributed control that is not specifically addressed at MPC, that uses static models, but with nonlinear equations, is, e.g., [8, 14, 15, 23]. In [14, 15] coordination is achieved by adjustment of common variables at an existing of fictitious border bus between the areas. In [8, 23] coordination is carried out by specified constraints, referred to as coupling constraints, that contain variables from multiple control areas. For both decomposition procedures, the controllers do not need to know the information of the whole system. Only peripheral data of each control area need to be exchanged between the controllers. The approach of [14, 15] has as drawback that it requires appropriate tuning of weighting factors in order to obtain adequate convergence speed. The approach of [8, 23] has as drawback that the coupling constraints for enforcing the coordination are not arrangeable for every type of system. It depends on the physical constraints of the network nodes at the border of each area, i.e., if they depend on neighboring network nodes or not.

Since the systems that we consider are governed by nonlinear equations, and since it is possible to set up coupling constraints for these systems, we propose here a distributed MPC approach, based on the work for static systems described in [8], that does explicitly take into account dynamics.

1.1.3 Outline

This chapter is outlined as follows. In Section 1.2 the concept of energy hubs is discussed in detail. A model representing producers, transmission infrastructures, energy hubs, and consumers is presented in Section 1.3. Section 1.4 introduces a centralized, MPC formulation for controlling energy hub systems, and in Section 1.5 we propose our distributed MPC approach. Simulation results applying the centralized as well as the distributed scheme to a three-hub system are presented in Section 1.6. Section 1.7 provides conclusions and directions for future research.

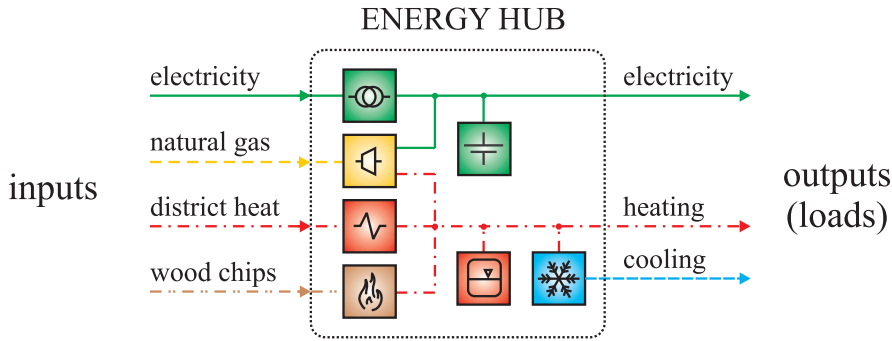


Fig. 1.3: Example of an energy hub containing a transformer, μ CHP, heat exchanger, furnace, absorption chiller, hot water storage, and battery.

1.2 Energy hub concept

Combining infrastructures means coupling them at certain nodes or branches, thereby enabling exchange of power between previously separated systems. As already mentioned, these couplings can be described by means of the energy hub concept. From a system point of view, an energy hub provides the functions of input, output, conversion, and storage of multiple energy carriers. An energy hub can thus be seen as a generalization or extension of a network node in an electrical network. An example of an energy hub is presented in Figure 1.3. Electricity, natural gas, district heat, and wood chips are consumed at the hub input and electricity, heating, and cooling is provided at the output port. For internal conversion and storage, the hub contains an electric transformer, a μ CHP device, a furnace, an absorption chiller, a battery, and a hot water storage.

Energy hubs contain three basic elements: direct connections, converters, and storage devices. Direct connections deliver an input carrier to the hub output without converting it into another form or without significantly changing its quality (e.g., voltage, pressure). Examples of this type of elements are electric cables and overhead lines as well as gas pipelines. Besides that, converter elements are used to transform an input energy carrier into another output carrier. Examples are steam and gas turbines, combustion engines, electric machines, fuel cells, etc. Compressors, pumps, transformers, power electronic inverters, heat exchangers, and other devices may be used for conditioning, i.e., for converting power into desirable qualities and quantities to be consumed by loads. Storage devices are incorporated within the hubs in order to store energy and to use it at a later instant or in order to preserve excessive heat produced by a μ CHP device. Examples are batteries for storing electric energy and hot water storages for conserving heat power.

The energy hub concept enables the integration of an arbitrary number of energy carriers and products (such as conversion and storage units) and thus provides high flexibility in system modeling. Co- or tri-generation power plants, industrial

plants (paper mills, refineries), big building complexes (airports, hospitals, shopping malls), as well as supply areas like urban districts or whole cities can all be modeled as energy hubs. In [12] the energy hub approach has been applied to a hydrogen network that includes converters (electrolyzer and fuel cell), storage, and demand. This hydrogen network is part of an integrated energy system with electricity, gas and heat production and demand.

Combining and coupling different energy carriers in energy hubs provides a number of potential benefits:

- **Flexibility of supply:** Load flexibility is increased, since redundant paths within the hub offer a certain degree of freedom in satisfying the output demand. This offers the potential for optimization.
- **Increased reliability:** Since the loads do not depend on one single infrastructure, the reliability of energy supply is increased [16].
- **Synergy effects:** Synergy effects among various energy carriers can be exploited by taking advantage of their complementary characteristics. E.g., electricity can be transmitted over long distances with relatively low losses. Chemical energy carriers such as natural gas can be stored using relatively simple and cheap technologies.

1.3 Modeling multi-carrier systems

Multi-carrier energy systems are modeled as an interconnection of several interconnected hubs. Accordingly, two cases are distinguished concerning the modeling. First, the equations for power flow *within* the hubs are presented. These equations incorporate the power conversion and the energy storage of the various energy carriers. Then, the equations concerning energy transmission *between* the hubs are given. Finally, the equations for the hub and the transmission network model are combined resulting in a complete model description.

1.3.1 System setup

In the system under study (Figure 1.4), each energy hub represents a general consumer, e.g., a household, that uses both electricity and gas. Each of the hubs has its own local electrical energy production (G_i , with electric power production $P_{e,i}^G$, for $i \in \{1, 2, 3\}$). Hub H_1 is connected to a large gas network N_1 , with gas infeed $P_{g,1}^G$. In addition, hub H_2 can obtain gas from a smaller gas network N_2 with limited capacity, modeled as gas infeed $P_{g,2}^G$. Each hub consumes electric power $P_{e,i}^H$ and gas $P_{g,i}^H$, and supplies energy to its electric load $L_{e,i}$ and its heat load $L_{h,i}$. The hubs contain converter and storage devices in order to fulfill their energy load requirements. For energy conversion, the hubs contain a μ CHP device and a furnace. The μ CHP

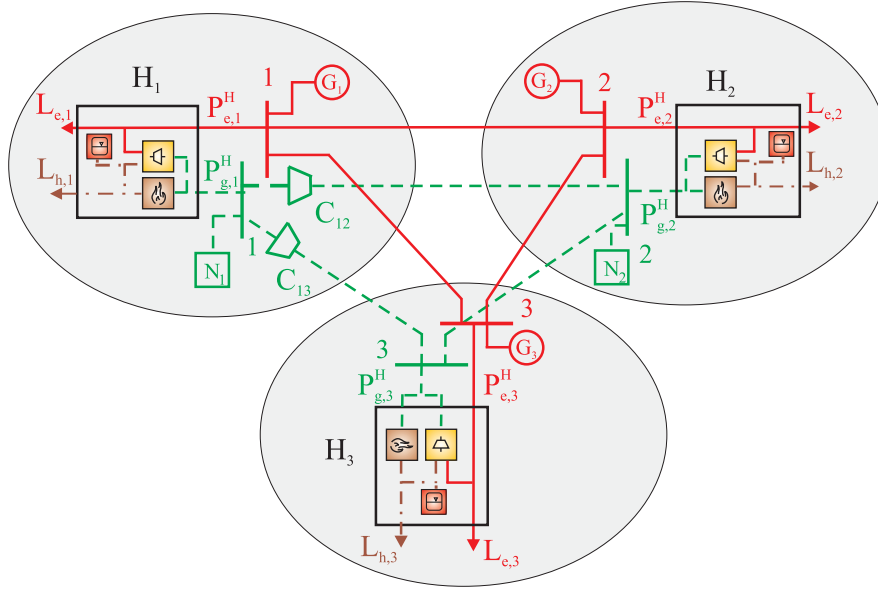


Fig. 1.4: System setup of three interconnected energy hubs. Active power is provided by generators G_1 , G_2 , G_3 . Hubs H_1 and H_2 have access to adjacent natural gas networks N_1 , N_2 .

device couples the two energy systems as it simultaneously produces electricity and heat from natural gas. All hubs additionally comprise a hot water storage device. Compressors (C_{ij} , for $(i, j) \in \{(1, 2), (1, 3)\}$) are present in the gas network within the pipelines originating from hub H_1 . The compressors provide a pressure decay and enable the gas flow from the large gas network to the surrounding gas sinks. As indicated in Figure 1.4, the entire network is divided into three control areas (grey circles), where each area (including hub and corresponding network nodes) is controlled by its respective control agent. A more detailed description of the control areas follows in Section 1.5.

Depending on the prices and load profiles, the μCHP device is utilized differently. At high electricity prices, the μCHP device is mainly operated according to the electric load. The heat produced simultaneously is then either used to supply the thermal load or stored in the heat storage device. At low electricity prices, the electric load is preferably supplied directly by the electricity network and the gas is used for supplying the thermal load via the furnace. Hence, there are several ways in which electric and thermal load demands can be fulfilled. This redundancy increases the reliability of supply and at the same time provides the possibility for optimizing the input energies, e.g., using criteria such as cost, availability, emissions, etc. [10, 16].

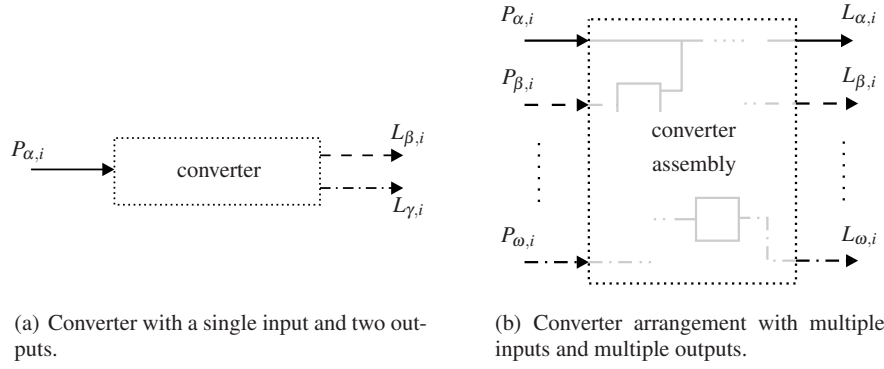


Fig. 1.5: Model of power converters with inputs $P_{\alpha,i}, P_{\beta,i}, \dots, P_{\omega,i}$ and outputs (loads) $L_{\alpha,i}, L_{\beta,i}, \dots, L_{\omega,i}$.

Since the operation of the system is examined over a longer time duration, the model is based on discrete time steps $k = 0, 1, \dots$, where a discrete time step k corresponds to the continuous time kT , where T corresponds to one hour.

1.3.2 Energy hub model

Here, the model of an energy hub is formalized, divided into a first part, describing the energy conversion, and into a second part, defining the energy storage models. The presented model is generic and can be applied to any configuration of converter and storage elements. The model is based on the assumption or simplification that within energy hubs, losses occur only in converter and storage elements. Furthermore, unidirectional power flows from the converter input to the converter output are implied. As an example, the hub equations for the energy hub depicted in Figure 1.4 are given.

1.3.2.1 Energy conversion

Within an energy hub i , power can be converted from one energy carrier α into another energy carrier β . We consider a single-input multiple-output converter device, as it is commonly the case in practical applications. Figure 5(a) illustrates a converter with two outputs, such as a micro turbine or gas turbine, producing electricity and heat by means of gas. The input power $P_{\alpha,i}(k)$ and output powers $L_{\beta,i}(k), L_{\gamma,i}(k)$ are at every time step k coupled as

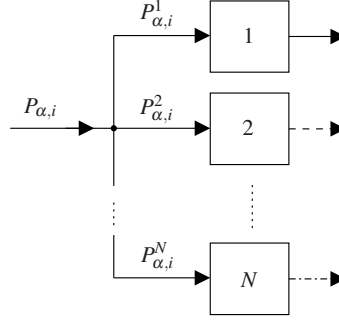


Fig. 1.6: Dispatch of total input power $P_{\alpha,i}$ to converters $c = 1, 2, \dots, N$.

$$L_{\beta,i}(k) = c_{\alpha\beta,i}(k)P_{\alpha,i}(k) \quad (1.1)$$

$$L_{\gamma,i}(k) = c_{\alpha\gamma,i}(k)P_{\alpha,i}(k), \quad (1.2)$$

where $c_{\alpha\beta,i}(k)$ and $c_{\alpha\gamma,i}(k)$ characterize the *coupling factors* between the input and output powers. In this case, the coupling factors correspond to the converter's steady-state energy efficiencies, denoted by $\eta_{\alpha\beta,i}$ and $\eta_{\alpha\gamma,i}$, respectively. More accurate converter models show non-constant efficiencies including the efficiency's dependency of the converted power level. This dependency can be incorporated by expressing the according coupling factor as a function of the converted power, i.e., $c_{\alpha\beta,i} = f_{\alpha\beta,i}(P_{\alpha,i}(k))$. As mentioned above, unidirectional power flows within the converters are assumed, i.e., $P_{\alpha,i}(k) \geq 0$, $P_{\beta,i}(k) \geq 0$, $P_{\gamma,i}(k) \geq 0$. Considering the entire hub (Figure 5(b)), various energy carriers and converter elements can be included, leading to the following relation:

$$\underbrace{\begin{bmatrix} L_{\alpha,i}(k) \\ L_{\beta,i}(k) \\ \vdots \\ L_{\omega,i}(k) \end{bmatrix}}_{\mathbf{L}_i(k)} = \underbrace{\begin{bmatrix} c_{\alpha\alpha,i}(k) & c_{\beta\alpha,i}(k) & \cdots & c_{\omega\alpha,i}(k) \\ c_{\alpha\beta,i}(k) & c_{\beta\beta,i}(k) & \cdots & c_{\omega\beta,i}(k) \\ \vdots & \vdots & \ddots & \vdots \\ c_{\alpha\omega,i}(k) & c_{\beta\omega,i}(k) & \cdots & c_{\omega\omega,i}(k) \end{bmatrix}}_{\mathbf{C}_i(k)} \underbrace{\begin{bmatrix} P_{\alpha,i}(k) \\ P_{\beta,i}(k) \\ \vdots \\ P_{\omega,i}(k) \end{bmatrix}}_{\mathbf{P}_i(k)}, \quad (1.3)$$

which expresses how the input powers $\mathbf{P}_i(k) = [P_{\alpha,i}(k), P_{\beta,i}(k), \dots, P_{\omega,i}(k)]^T$ are converted into the output powers $\mathbf{L}_i(k) = [L_{\alpha,i}(k), L_{\beta,i}(k), \dots, L_{\omega,i}(k)]^T$. Matrix $\mathbf{C}_i(k)$ is referred to as the coupling matrix and is directly derived from the hub's converter structure and the converter's efficiency characteristics. Equation (1.3) illustrates a general formulation of a multi-input multi-output converter device. In reality, not every energy carrier is occurring at the input as well as at the output port. Moreover, the number of inputs and outputs do not have to coincide.

As the input powers $\mathbf{P}_i(k)$ can be distributed among various converter devices, so-called *dispatch factors* specify how much power goes into the corresponding

converter device. Figure 1.6 outlines the concept, where the input carrier $P_{\alpha,i}(k)$ is divided over N converter devices as input carriers $P_{\alpha,i}^c$ ($c = 1, \dots, N$),

$$P_{\alpha,i}^c(k) = v_{\alpha,i}^c(k) P_{\alpha,i}(k). \quad (1.4)$$

The conservation of power introduces the constraints

$$0 \leq v_{\alpha,i}^c(k) \leq 1 \quad \forall \alpha, \forall c \quad (1.5)$$

$$\sum_{c=1}^N v_{\alpha,i}^c(k) = 1 \quad \forall \alpha. \quad (1.6)$$

Hence, the coupling factors $c_{\alpha\beta,i}(k)$ for converters without explicitly preassigned inputs are defined as the product of dispatch factor and converter efficiency, i.e., $c_{\alpha\beta,i}(k) = v_{\alpha,i}^c(k) \eta_{\alpha\beta,i}$.

As long as the converter efficiencies are assumed to be constant, (1.3) represents a linear transformation. Including the power dependency as $c_{\alpha\beta,i}(k) = f_{\alpha\beta,i}(P_{\alpha,i}(k))$ results in a nonlinear relation. In either case, different inputs powers $\mathbf{P}_i(k)$ can be found that fulfill the load requirements $\mathbf{L}_i(k)$ at the output, since the dispatch factor $v(k)$ is variable. This reflects the degrees of freedom in supply which are used for optimization.

Application example

The hub equations for power conversion are now derived for the exemplary hubs in Figure 1.4. The electrical load $L_{e,i}(k)$ and the heat load $L_{h,i}(k)$ at a time step k are related to the electricity $P_{e,i}^H(k)$ and gas hub input $P_{g,i}^H(k)$ as follows:

$$\underbrace{\begin{bmatrix} L_{e,i}(k) \\ L_{h,i}(k) \end{bmatrix}}_{\mathbf{L}_i(k)} = \underbrace{\begin{bmatrix} 1 & v_{g,i}(k) \eta_{ge,i}^{\text{CHP}} \\ 0 & v_{g,i}(k) \eta_{gh,i}^{\text{CHP}} + (1 - v_{g,i}(k)) \eta_{gh,i}^{\text{F}} \end{bmatrix}}_{\mathbf{C}_i(k)} \underbrace{\begin{bmatrix} P_{e,i}^H(k) \\ P_{g,i}^H(k) \end{bmatrix}}_{\mathbf{P}_i(k)}, \quad (1.7)$$

for $i = 1, 2, 3$, where $\eta_{ge,i}^{\text{CHP}}$ and $\eta_{gh,i}^{\text{CHP}}$ denote the gas-electric and gas-heat efficiencies of the μCHP device and where $\eta_{gh,i}^{\text{F}}$ denotes the efficiency of the furnace. The variable $v_{g,i}(k)$ ($0 \leq v_{g,i}(k) \leq 1$) represents the dispatch factor that determines how the gas is divided between the μCHP and the furnace. The term $v_{g,i}(k) P_{g,i}^H(k)$ defines the gas input power fed into the μCHP , and according to (1.6) the part $(1 - v_{g,i}(k)) P_{g,i}^H(k)$ defines the gas input power going into the furnace. (Since the gas dispatch involves only two converter devices, the superscript c indicating the correspondent converter, is omitted.)

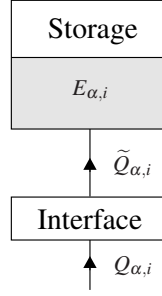


Fig. 1.7: Storage element exchanging the power $Q_{\alpha,i}$; internal power $\tilde{Q}_{\alpha,i}$, stored energy $E_{\alpha,i}$.

1.3.2.2 Energy storage

The storage device is modeled as an ideal storage in combination with a storage interface [9](Figure 1.7). The relation between the power exchange $Q_{\alpha,i}(k)$ and the effectively stored energy $E_{\alpha,i}(k)$ at time step k is defined by the following equation:

$$\begin{aligned} Q_{\alpha,i}(k) &= \frac{\dot{E}_{\alpha,i}}{e_{\alpha,i}} = \frac{1}{e_{\alpha,i}} \frac{dE_{\alpha,i}}{dt} \approx \frac{1}{e_{\alpha,i}} \frac{\Delta E_{\alpha,i}}{\Delta t} \\ &= \frac{1}{e_{\alpha,i}} \left(\frac{E_{\alpha,i}(k) - E_{\alpha,i}(k-1)}{\Delta t} + \dot{E}_{\alpha,i}^{\text{stb}} \right), \end{aligned} \quad (1.8)$$

with

$$e_{\alpha,i} = \begin{cases} e_{\alpha,i}^+ & \text{if } Q_{\alpha,i}(k) \geq 0 \quad (\text{charging/standby}) \\ 1/e_{\alpha,i}^- & \text{else} \quad (\text{discharging}), \end{cases} \quad (1.9)$$

where $e_{\alpha,i}^+$, $e_{\alpha,i}^-$ are the charging and discharging efficiencies of the heat storage device, respectively, including the efficiency of the storage interface, converting the energy carrier exchanged with the system $Q_{\alpha,i}(k)$ into the carrier stored internally $\tilde{Q}_{\alpha,i}(k)$, according to $\tilde{Q}_{\alpha,i}(k) = e_{\alpha,i} Q_{\alpha,i}(k)$. The storage energy at time step k is denoted by $E_{\alpha,i}(k)$, and $\dot{E}_{\alpha,i}^{\text{stb}}$ represents the standby energy losses of the heat storage device per period ($\dot{E}_{\alpha,i}^{\text{stb}} \geq 0$).

Depending on which side of the converter the storage device is located, the following power flow equations result. Figure 1.8 illustrates the situation. If the storage is located at the input side of the converter devices the power flow equations are described by

$$\tilde{P}_{\alpha,i}(k) = P_{\alpha,i}(k) - Q_{\alpha,i}(k), \quad (1.10)$$

and if the storage is placed at the output side of to the converter device, the equations are given by

$$\tilde{L}_{\beta,i}(k) = L_{\beta,i}(k) + M_{\beta,i}(k), \quad (1.11)$$

where $M_{\beta,i}(k)$ denotes the storage flow of a storage device at the output side of a converter, analogously to $Q_{\alpha,i}(k)$. Examples of storages before the converter devices are gas storages before a μ CHP device or hydrogen storages before fuel cells. The hydrogen storage is filled by an electrolyzer, converting electricity into hydrogen. Storage examples after converters are heat storages after heat exchangers or μ CHP devices or the above mentioned hydrogen storages after electrolyzers.

When merging all power flows, the inputs and outputs of the entire hub are then described by

$$\left[\mathbf{L}_i(k) + \mathbf{M}_i(k) \right] = \mathbf{C}_i(k) \left[\mathbf{P}_i(k) - \mathbf{Q}_i(k) \right], \quad (1.12)$$

where $\mathbf{Q}_{\alpha,i}(k)$ and $\mathbf{M}_{\alpha,i}(k)$ state all input-side and output-side storage power flows.

Here, we assume the converter efficiencies to be constant, i.e., to be independent of the converted power level, which results in a constant coupling matrix $\mathbf{C}_i(k)$ for each time step k . We can then apply superposition and summarize all storage flows in an equivalent output storage flow vector

$$\mathbf{M}_i^{\text{eq}}(k) = \mathbf{C}_i(k) \mathbf{Q}_i(k) + \mathbf{M}_i(k). \quad (1.13)$$

With (1.8) and (1.13), the storage flows and the storage energy derivatives are related by

$$\underbrace{\begin{bmatrix} M_{\alpha,i}^{\text{eq}}(k) \\ \vdots \\ M_{\omega,i}^{\text{eq}}(k) \end{bmatrix}}_{\mathbf{M}_i^{\text{eq}}(k)} = \underbrace{\begin{bmatrix} s_{\alpha\alpha,i}(k) & \cdots & s_{\omega\alpha,i}(k) \\ \vdots & \ddots & \vdots \\ s_{\alpha\omega,i}(k) & \cdots & s_{\omega\omega,i}(k) \end{bmatrix}}_{\mathbf{S}_i(k)} \underbrace{\begin{bmatrix} \dot{E}_{\alpha,i}(k) \\ \vdots \\ \dot{E}_{\omega,i}(k) \end{bmatrix}}_{\dot{\mathbf{E}}_i(k)}, \quad (1.14)$$

where the *storage coupling matrix* $\mathbf{S}_i(k)$ describes how changes within the storage energies affect the output flows, i.e., how the storage energy derivatives are mapped into equivalent output-side flows. According to (1.8), the storage energy derivatives correspond to

$$\dot{\mathbf{E}}_i(k) = \mathbf{E}_i(k) - \mathbf{E}_i(k-1) + \dot{\mathbf{E}}_i^{\text{stb}}. \quad (1.15)$$

Adding the storage equation 1.14 to the general hub equation yields the following flows through an energy hub:

$$\mathbf{L}_i(k) + \mathbf{S}_i(k) \dot{\mathbf{E}}_i(k) = \mathbf{C}_i(k) \mathbf{P}_i(k). \quad (1.16)$$

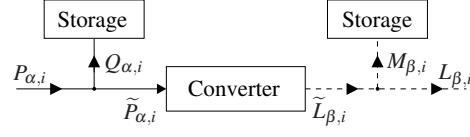


Fig. 1.8: $\alpha\beta$ -converter with α -storage at the input and β -storage at the output.

Application example

For each hub depicted in Figure 1.4, hot water storage devices are implemented. Equation (1.7) is therefore completed with additional storage power flows, which are collected in a vector $\mathbf{M}_i(k)$:

$$\underbrace{\begin{bmatrix} L_{e,i}(k) \\ L_{h,i}(k) + M_{h,i}(k) \end{bmatrix}}_{\mathbf{L}_i(k) + \mathbf{M}_i(k)} = \underbrace{\begin{bmatrix} 1 & v_{g,i}(k)\eta_{ge,i}^{\text{CHP}} \\ 0 & v_{g,i}(k)\eta_{gh,i}^{\text{CHP}} + (1 - v_{g,i}(k))\eta_{gh,i}^{\text{F}} \end{bmatrix}}_{\mathbf{C}_i(k)} \underbrace{\begin{bmatrix} P_{e,i}^{\text{H}}(k) \\ P_{g,i}^{\text{H}}(k) \end{bmatrix}}_{\mathbf{P}_i(k)}. \quad (1.17)$$

1.3.3 Transmission model

As introduced above, we consider here a system where the hubs are interconnected by two types of transmission systems, an electricity and a natural gas network. However, district heating systems or hydrogen systems are also possible transmission systems for interconnecting hubs. For the transmission networks of both the electricity network and the gas pipeline network, power flow models based on nodal power balances are implemented.

1.3.3.1 AC electricity network

Electric power flows are formulated as nodal power balances of the complex power, according to the normal power flow equations [17]. At node m , the complex power balance at time step k is stated as

$$S_m(k) - \sum_{n \in N_m} S_{mn}(k) = 0, \quad (1.18)$$

where $S_m(k)$ is the complex power injected at node m , and $S_{mn}(k)$ denotes the power flow to all adjacent nodes n of node m , summarized in the set N_m . The line flows are expressed by the voltage magnitudes $V(k)$ and angles $\theta(k)$ and the line parameters:

$$S_{mn}(k) = y_{mn}^* V_m(k) e^{j\theta_m(k)} (V_m(k) e^{-j\theta_m(k)} - V_n(k) e^{-j\theta_n(k)}) - j b_{mn}^{\text{sh}} V_m^2(k), \quad (1.19)$$

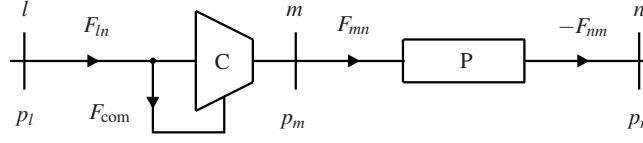


Fig. 1.9: Model of a gas pipeline with compressor (C) and pipeline (P). Compressor demand is modeled as additional gas flow F_{com} .

where the superscript $*$ denotes the conjugate complex of the value. The line is modeled as a π -equivalent with the series admittance y_{mn} and the shunt susceptance b_{mn}^{sh} [17].

1.3.3.2 Pipeline network

Figure 1.9 shows the model of a gas pipeline composed of a compressor and a pipeline element. The volume flow balance at node m at time step k is defined as

$$F_m(k) - \sum_{n \in \mathcal{N}_m} F_{mn}(k) = 0, \quad (1.20)$$

where $F_m(k)$ is the volume flow injected at node m , $F_{mn}(k)$ denotes the line flow between nodes m and n , and \mathcal{N}_m denotes the set of neighboring nodes of node m , i.e., the nodes connected to node m through a pipeline. The line flow $F_{mn}(k)$ can be calculated as

$$F_{mn}(k) = k_{mn} s_{mn} \sqrt{s_{mn} (p_m^2(k) - p_n^2(k))}, \quad (1.21)$$

where $p_m(k)$ and $p_n(k)$ denote the upstream and downstream pressures, respectively, and k_{mn} identifies the line constant. The variable s_{mn} indicates the direction of the gas flow as

$$s_{mn} = \begin{cases} +1 & \text{if } p_m(k) \geq p_n(k) \\ -1 & \text{otherwise.} \end{cases} \quad (1.22)$$

The pipeline flow equation (1.21) is for most purposes a good approximation for all types of isothermal pipeline flows (liquid and gaseous). For obtaining more precise results for specific fluids and flow conditions a number of modified equations are available in [20].

To maintain a certain pressure level a compressor is needed. Here, the compressor is driven by a gas turbine which is modeled as additional gas flow

$$F_{\text{com}}(k) = k_{\text{com}} F_{mn}(k) (p_m(k) - p_l(k)), \quad (1.23)$$

where $p_l(k)$ and $p_m(k)$ denote the pressures at the compressor input and output side, respectively, and k_{com} is a compressor constant. Basically, the amount of power consumed by the compressor depends on the pressure added to the fluid and on the volume flow rate through it. The resulting gas flow into the pipeline $F_{mn}(k)$ is therefore determined by

$$F_{mn}(k) = F_{ln}(k) - F_{\text{com}}(k). \quad (1.24)$$

The pressure at the compressor output $p_m(k)$ is determined by

$$p_m(k) = p_{\text{inc}}(k)p_l(k), \quad (1.25)$$

where $p_{\text{inc}}(k)$ defines the pressure amplification of the compressor. Depending on the required line flow $F_{mn}(k)$, $p_{\text{inc}}(k)$ is adjusted accordingly. For the purpose of this study, these simplified compressor models provide sufficient accuracy. More advanced compressor equations taking into account changing fluid properties are given in [20].

The volume flow rate $F_{mn}(k)$ corresponds to a power flow $P_{g,mn}(k)$. The relation between volume and power flow is described by

$$P_{g,mn}(k) = c_{\text{GHV}}F_{mn}(k), \quad (1.26)$$

where c_{GHV} is the gross heating value of the fluid. The gross heating value depends on the fluid and is given in MWh/m^3 . Values of different fluids can be found in [20].

1.3.4 Complete model description

The combined hub and transmission network model is obtained by combining the power flow models stated above. The system setup in Figure 1.4 serves again as example. For each time step k , the following three vectors are defined:

- algebraic state vector $\mathbf{z}(k)$: The algebraic state vector includes the variables for which no explicit dynamics are defined:

$$\mathbf{z}(k) = [\mathbf{V}^T(k), \boldsymbol{\theta}^T(k), \mathbf{p}^T(k), \mathbf{p}_{\text{inc}}^T(k), (\mathbf{P}_e^H)^T(k), (\mathbf{P}_g^H)^T(k)]^T, \quad (1.27)$$

where

- $\mathbf{V}(k) = [V_1(k), V_2(k), V_3(k)]^T$ and $\boldsymbol{\theta}(k) = [\theta_1(k), \theta_2(k), \theta_3(k)]^T$ denote the voltage magnitudes and angles of the electric buses, respectively,
- $\mathbf{p}(k) = [p_1(k), p_2(k), p_3(k)]^T$ denotes the nodal pressures of all gas buses,
- $\mathbf{p}_{\text{inc}}(k) = [p_{\text{inc},1}(k), p_{\text{inc},2}(k)]^T$ denotes the pressure amplification of the compressors,
- $\mathbf{P}_e^H(k) = [P_{e,1}^H(k), P_{e,2}^H(k), P_{e,3}^H(k)]^T$ denotes the electric inputs of the hubs, and
- $\mathbf{P}_g^H(k) = [P_{g,1}^H(k), P_{g,2}^H(k), P_{g,3}^H(k)]^T$ denotes the gas inputs of the hubs.

- dynamic state vector $\mathbf{x}(k)$: The dynamic state vector includes variables for which dynamics are included:

$$\mathbf{x}(k) = \mathbf{E}_h(k), \quad (1.28)$$

where

- $\mathbf{E}_h(k) = [E_{h,1}(k), E_{h,2}(k), E_{h,3}(k)]^T$ denotes the energy contents of the heat storage devices.

- control vector $\mathbf{u}(k)$: The control variables include the operational set-points of the system:

$$\mathbf{u}(k) = \left[(\mathbf{P}_e^G)^T(k), (\mathbf{P}_g^G)^T(k), \mathbf{v}_g^T(k) \right]^T, \quad (1.29)$$

where

- $\mathbf{P}_e^G(k) = [P_{e,1}^G(k), P_{e,2}^G(k), P_{e,3}^G(k)]^T$ denotes the active power generation of all generators,
- $\mathbf{P}_g^G(k) = [P_{g,1}^G(k), P_{g,2}^G(k)]^T$ defines the natural gas imports and
- $\mathbf{v}_g(k) = [v_{g,1}(k), v_{g,2}(k), v_{g,3}(k)]^T$ describes the dispatch factors of the gas input junctions.

Now, the model that we use to represent the multi-carrier network, including the hub equations with the dynamics, can be written in compact form as

$$\mathbf{x}(k+1) = \mathbf{f}(\mathbf{x}(k), \mathbf{z}(k), \mathbf{u}(k)) \quad (1.30)$$

$$\mathbf{0} = \mathbf{g}(\mathbf{x}(k), \mathbf{z}(k), \mathbf{u}(k)). \quad (1.31)$$

Equation (1.30) represent the difference equations describing the dynamics in the system, i.e., the dynamics in the storage devices. The equality constraints (1.31) represent the static, instantaneous relations in the system, i.e., the transmission and energy conversion components of the system.

1.4 Centralized model predictive control

One way to determine the actions that yield the optimal operation of the system is by using centralized control. In centralized control, a centralized controller measures all variables in the network and determines actions or set-points for all actuators, i.e., the energy generation units, converters, and storage devices. We propose to use a model-based predictive control (MPC) scheme to determine the control variables $\mathbf{u}(k)$ in such a way that the total operational costs of the system are minimized while satisfying the system constraints. Below, we explain the basic idea of MPC. Then, the MPC problem for the considered hub system is formulated for centralized control.

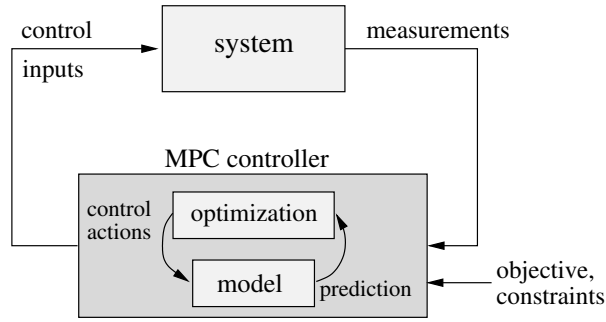


Fig. 1.10: Illustration of model predictive control.

1.4.1 Principle of operation

MPC [6, 19] is an optimization-based control strategy where an optimization problem is solved at each discrete decision step. This optimization problem uses an internal prediction model to find those actions that give the best predicted system behavior over a certain prediction horizon with length N . In this optimization operational constraints are also taken into account. MPC operates in a receding horizon fashion, meaning that at each time step new measurements of the system and new predictions into the future are made and new control actions are computed. By using MPC, actions can be determined that anticipate future events, such as increasing or decreasing energy prices or changes within the load profiles. MPC is suited for control of multi-carrier systems, since it can adequately take into account the dynamics of the energy storage devices and the characteristics of the electricity and gas networks.

In Figure 1.10 the operation of an MPC scheme is illustrated schematically. At each discrete control step k , an MPC controller first measures the current state of the system, $\mathbf{x}(k)$. Then, it computes which control input $\mathbf{u}(k)$ to be provided to the system, by using (numerical) optimization to determine the actions that give the best predicted performance over a prediction horizon of N time steps as defined by an objective function. The control variables computed for the first prediction step are then applied to the physical system. The system then transitions to a new state, $\mathbf{x}(k+1)$, after which the above procedure is repeated.

1.4.2 Problem formulation

In the MPC formulation the central controller determines the inputs $\mathbf{u}(k)$ for the network by solving the following optimization problem:

$$\min_{\tilde{\mathbf{u}}(k)} J(\tilde{\mathbf{x}}(k+1), \tilde{\mathbf{z}}(k), \tilde{\mathbf{u}}(k)) \quad (1.32)$$

subject to

$$\tilde{\mathbf{x}}(k+1) = \tilde{\mathbf{f}}(\tilde{\mathbf{x}}(k), \tilde{\mathbf{z}}(k), \tilde{\mathbf{u}}(k)) \quad (1.33)$$

$$\tilde{\mathbf{g}}(\tilde{\mathbf{x}}(k), \tilde{\mathbf{z}}(k), \tilde{\mathbf{u}}(k)) = \mathbf{0} \quad (1.34)$$

$$\tilde{\mathbf{h}}(\tilde{\mathbf{x}}(k), \tilde{\mathbf{z}}(k), \tilde{\mathbf{u}}(k)) \leq \mathbf{0}, \quad (1.35)$$

where the tilde over a variable represents a vector with the values of this variable over a prediction horizon of N steps, e.g., $\tilde{\mathbf{u}}(k) = [\mathbf{u}^T(k), \dots, \mathbf{u}^T(k+N-1)]^T$.

For the system setup under consideration, i.e., the system in Figure 1.4, the control objective is to minimize the energy costs, i.e., the costs for electricity energy and natural gas. The following objective function will be used in this minimization, in which costs of the individual energy carriers are modeled as quadratic functions of the corresponding powers:

$$J = \sum_{l=0}^{N-1} \sum_{i \in G} q_i^G(k+l) (P_{e,i}^G(k+l))^2 + q_i^N(k+l) (P_{g,i}^G(k+l))^2, \quad (1.36)$$

where G is a set of generation unit indices, i.e., the three generators and the two natural gas providers. The prices for active power generation $q_i^G(k)$ and for natural gas consumption $q_i^N(k)$ can vary throughout the day.

The equality constraints (1.33) and (1.34) represent the dynamic and static relations of the prediction model of the system. They correspond to equations (1.30) and (1.31), formulated over the prediction horizon N . The inequality constraints (1.35) comprise limits on the voltage magnitudes, active and reactive power flows, pressures, changes in compressor settings, and dispatch factors. Furthermore, power limitations on hub inputs and on gas and electricity generation are also incorporated into (1.35). Regarding the storage devices, limits on storage contents and storage flows are imposed.

The optimization problem (1.32)–(1.35) is a nonlinear programming problem [4], which can be solved using solvers for nonlinear programming, such as sequential quadratic programming [4]. In general, the solution space is nonconvex and therefore finding a global optimum cannot be guaranteed. Unless a multi-start approach with a sufficient number of starts is used, a local optimum is returned by the numerical optimization.

1.5 Distributed model predictive control

Although a centralized controller could in theory give the best performance, practical and computational limitations prevent such a centralized controller from being useful in practice. The overall network may be owned by different entities, and these different entities may not want to give access to their sensors and actuators to

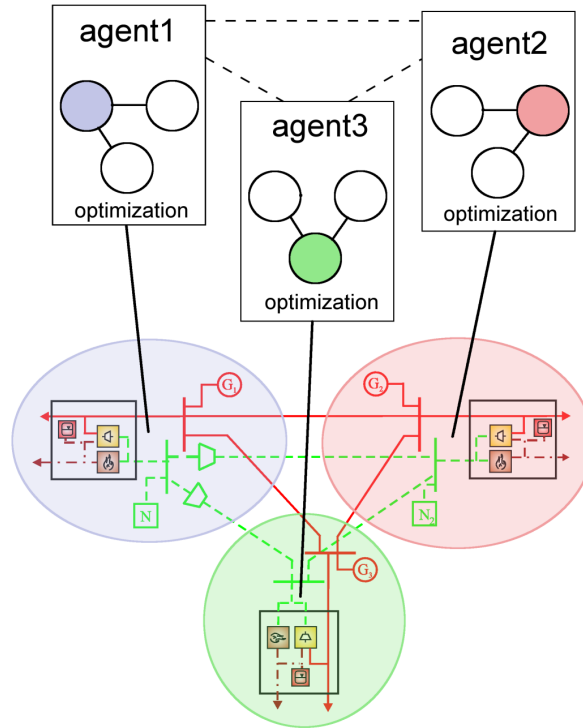


Fig. 1.11: Three-hub system controlled by three communicating agents.

a centralized authority. Even if they would allow a centralized authority to take over control of their part of the network, this centralized authority would have computational problems solving the resulting centralized control problem due to its large size. In that case, it has to be accepted that several different MPC controllers are present, each controlling their own parts of the network, e.g., their own households.

Figure 1.11 shows the introduced three-hub system controlled by three agents. Each agent, or controller, solves its own local MPC problem using the local model of its part of the system. However, the solution of a local MPC problem depends on the solution of the MPC problems of the surrounding MPC controllers, since the electricity and gas networks interconnect the hubs. Therefore, the MPC problems of the controllers have to be solved in a cooperative way by allowing communication between the agents (dashed lines in Figure 1.11). This is not only to ensure that the controllers choose feasible actions, but also to allow the controllers to choose actions that are optimal from a system-wide point of view.

In our application, the MPC subproblems are based on nonlinear dynamic models. We therefore propose an extension of the static distributed control scheme in [8] that does take into account dynamics. Hence, the method is extended for optimiza-

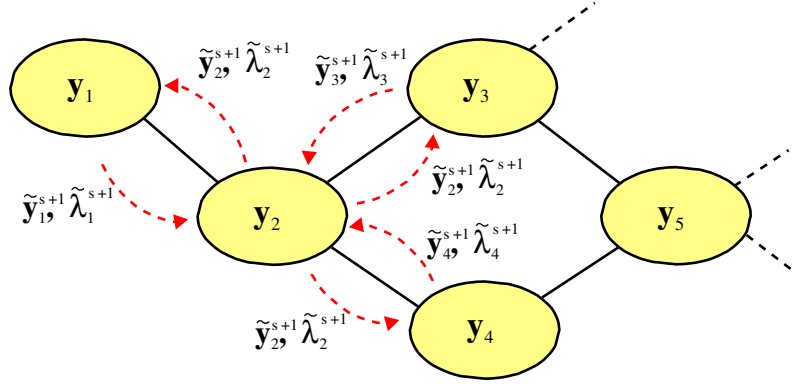


Fig. 1.12: Coordination procedure between multiple interconnected areas by exchanging system variables \mathbf{y} and Lagrangian multipliers λ .

tion over multiple time steps in an MPC way. We then obtain an approach based on a combination of MPC and Lagrangian relaxation.

1.5.1 Principle of operation

Here, we explain the mathematical concept to decompose a general MPC optimization problem into several subproblems for individual distributed controllers. The procedure is presented on an interconnected multi-area system depicted in Figure 1.12. The areas $a = 1, 2, \dots, A$ are interconnected in an arbitrary way. The system variables of each area a comprise the algebraic state vector $\tilde{\mathbf{z}}_a(k)$ and dynamic state vector $\tilde{\mathbf{x}}_a(k)$ as well as the control variables $\tilde{\mathbf{u}}_a(k)$, i.e.,

$$\tilde{\mathbf{y}}_a(k) = [\tilde{\mathbf{x}}_a(k), \tilde{\mathbf{z}}_a(k), \tilde{\mathbf{u}}_a(k)]^T \quad \text{for } a = 1, \dots, A. \quad (1.37)$$

The overall, centralized MPC optimization problem can then be defined as

$$\min_{\tilde{\mathbf{u}}_a(k)} \sum_{a=1}^A J_a(\tilde{\mathbf{y}}_a(k)) \quad (1.38)$$

$$\text{subject to } \tilde{\mathbf{g}}(\tilde{\mathbf{y}}_a(k)) = \mathbf{0} \quad \text{for } a = 1, \dots, A \quad (1.39)$$

$$\hat{\tilde{\mathbf{g}}}_a(\tilde{\mathbf{y}}_1(k), \dots, \tilde{\mathbf{y}}_a(k), \dots, \tilde{\mathbf{y}}_A(k)) = \mathbf{0} \quad \text{for } a = 1, \dots, A, \quad (1.40)$$

where only equality constraints are included for the sake of demonstration. Inequality constraints are handled analogously. The constraints are classified into two types of constraints. Constraints that involve only the local system variables are collected in (1.39). Besides these purely local constraints, so-called *coupling constraints* (1.40) (marked by a hat) are present, containing variables from multiple control areas. These coupling constraints are related to multiple areas and thus pre-

vent the controllers of each subsystem from operating independently of each other. These constraints are the reason why coordination between the controllers is necessary.

1.5.1.1 Decomposition methodology

For decomposing this centralized MPC optimization problem into optimization problems for the controllers of the individual control areas, both the objective and the equality constraints are separated and assigned to a responsible control agent.

The constraints (1.39) with only local variables are assigned to the corresponding controller of each area. The coupling constraints (1.40) can in principle be assigned arbitrarily to the controllers. However, they are assigned to the area that contains the majority of the coupling variables. Coupling variables are the variables of the peripheral buses, also referred to as border buses, which are buses that are directly connected to buses of another area.

The subproblems for the individual controllers are now obtained by relaxing some of the coupling constraints and adding them to the objectives of the different controllers. Conventional Lagrangian relaxation is based on relaxing the own coupling constraints of each controller by incorporating them into their objective functions [15], weighted by Lagrangian multipliers. The obtained subproblems are then solved in a series of iterations, where each local optimization problem is solved with fixed values for the variables of the other controllers. After each iteration the Lagrangian multipliers are updated with a sub-gradient method. To avoid this update, which requires appropriate tuning of the update parameters, an advanced method establishes the subproblems by relaxing the coupling constraints assigned to the foreign areas (modified Lagrangian relaxation procedure [8]).

The resulting subproblem for each area $a = 1, \dots, A$ is then formally written as

$$\min_{\tilde{\mathbf{u}}_a(k)} J_a(\tilde{\mathbf{y}}_a(k)) + \sum_{b=1, b \neq a}^A (\tilde{\lambda}_b^s)^T \tilde{\mathbf{g}}_b(\tilde{\mathbf{y}}^a(k)) \quad (1.41)$$

$$\text{subject to } \tilde{\mathbf{g}}_a(\tilde{\mathbf{y}}_a(k)) = \mathbf{0}, \quad (1.42)$$

$$\tilde{\mathbf{g}}_a(\tilde{\mathbf{y}}^a(k)) = \mathbf{0}, \quad (1.43)$$

where $\tilde{\mathbf{y}}^a(k) = [\tilde{\mathbf{y}}_1^s(k), \dots, \tilde{\mathbf{y}}_a(k), \dots, \tilde{\mathbf{y}}_A^s(k)]$ represents the system variables of all neighboring areas of area a . λ are the Lagrangian multipliers which will be explained below. The superscript s indicates the iteration step. As mentioned above, the optimization problems of the individual control agents are solved in an iterative procedure, keeping the variables of the neighboring areas constant. Both, the objective and the coupling constraints depend on variables of the foreign areas, referred to foreign variables, indicated by the superscript s .

The objective function of each controller consists of two parts. The first term expresses the main objective originating from the overall objective function (1.38). The second term is responsible for the coordination between the agents and consists

of the coupling constraints introduced above. As indicated in (1.41) - (1.43), the coupling constraints of the own area are kept explicitly as hard constraints of the constraint set of the own controller (1.43) and are then added as soft constraints to the main objective of the other controllers. This follows the principle of the modified Lagrangian relaxation procedure [24]. The weighting factors of the soft constraints are the Lagrangian multipliers obtained from the optimization problem of the neighboring controllers.

1.5.1.2 Solution scheme

Both the objectives and the coupling constraints depend on variables of multiple controllers. To handle this dependency, the optimization problems of the controllers are solved in an iterative procedure:

- At each iteration step s , the MPC optimization problems of all control agents are solved independently of each other, while keeping the variables of the other controllers constant.
- After each iteration, the controllers exchange the updated values of their variables, i.e., the variables $\tilde{\mathbf{y}}_i^{s+1}(k)$ and the Lagrange multipliers $\tilde{\lambda}_i^{s+1}(k)$, where i refers to the corresponding control area. Figure 1.12 indicates the dependencies between area 2 and its surrounding areas. Only the variables between two directly connected areas need to be exchanged. Thus, area 5 does not need to send its variables to area 2.
- Convergence is achieved when the exchanged variables do not change more than a small tolerance γ_{tol} in two consecutive iterations.

Note that not the whole set of the updated system variables needs to be exchanged between the areas. Only the updated coupling variables have to be exchanged. For the sake of clarity of notation, the system variables and the effectively exchanged variables are not distinguished in the notation. In contrary to conventional Lagrangian relaxation procedures, a faster convergence is achieved as the weighting factors are represented by the Lagrangian multipliers of the neighboring optimization problem [24].

1.5.2 Application

We next apply the decomposition procedure to our three-hub system, as depicted in Figure 1.4. It is noted that although here we only consider three hubs, the presented decomposition procedure is also suited for large-scale systems. The considered three-hub network is divided into three control areas, according to the hubs. Each of the control areas has a controller for determining the local control actions.

1.5.2.1 Local variables

The controller of a particular hub considers as its variables the hub variables and the system variables of the nodes connected to it. For example, for the first controller, the state and control vectors for each time step k are defined as

$$\mathbf{x}_1(k) = E_{h,1}(k) \quad (1.44)$$

$$\mathbf{z}_1(k) = [V_1(k), \theta_1(k), p_1(k), p_{inc,1}(k), p_{inc,2}(k), P_{e,1}^H(k), P_{g,1}^H(k)]^T \quad (1.45)$$

$$\mathbf{u}_1(k) = [P_{e,1}^G(k), P_{g,1}^G(k), v_{g,1}(k)]^T. \quad (1.46)$$

The state and control vectors for the second and third controller are defined similarly according to Figure 1.4.

1.5.2.2 Objective functions

Each individual controller has its own control objective. In particular, the objective functions of the three controllers are:

$$J_1 = \sum_{l=0}^{N-1} q_1^G(k+l)(P_{e,1}^G(k+l))^2 + q_1^N(k+l)(P_{g,1}^G(k+l))^2 \quad (1.47)$$

$$J_2 = \sum_{l=0}^{N-1} q_2^G(k+l)(P_{e,2}^G(k+l))^2 + q_2^N(k+l)(P_{g,2}^G(k+l))^2 \quad (1.48)$$

$$J_3 = \sum_{l=0}^{N-1} q_3^G(k+l)(P_{e,3}^G(k+l))^2. \quad (1.49)$$

1.5.2.3 Coupling constraints

The three optimization problems have to be coordinated by adding the respective coupling constraints to the individual objectives given above. Below, the coupling constraints for the electric power and for the gas transmission systems are presented. Then, the resulting objectives are formulated.

Electric power systems

For applying the procedure to electric power systems, the constraints are arranged in the following way. The power flow equations of all inner buses of a particular area are incorporated into the equality constraints $\tilde{\mathbf{g}}_A(\tilde{\mathbf{y}}_A(k)) = 0$, $\tilde{\mathbf{g}}_B(\tilde{\mathbf{y}}_B(k)) = 0$. Inner buses are those buses of an area that have at least one bus in between themselves and the buses of another area. Buses that are directly connected to buses of another area are referred to as peripheral buses or border buses.

Regarding the couplings, the electric power flow equations at the border buses serve as coupling constraints. A coupling between the areas is only enabled when these power flow equations comprehend variables of both areas. This implies that the constraints for the active and reactive power balance serve as coupling constraints, but not the equations regarding voltage magnitude and angle reference settings. Hence, having PQ buses (active and reactive power are specified [17]) at the common tie-lines results in two coupling constraints per peripheral bus. A less tight coupling is achieved with PV buses (active power and voltage magnitude are specified [17]), yielding only one coupling constraint. If the slack bus (voltage magnitude and voltage angle are specified [17]) is situated at one of the border buses, the procedure is not implementable, because only voltage magnitude and angle reference settings have to hold for these kind of buses. For the case of active power control, the slack bus is modeled as a PV bus with an additional angle reference in order to obtain enough coupling constraints. The inequality constraints are occurring with transmission limits on tie-lines belonging to both areas. To classify the inequality constraints into own and foreign constraints the tie-lines need to be allocated to one area, arbitrarily.

For the studied three-hub system, the active power balances of all nodes of the electricity system require coordination as they depend on the neighboring voltage magnitudes and angles. For each coupling constraint, the dependencies of the own and foreign system variables (marked by superscript s , which specifies the current iteration step) are indicated. Since each node serves as border bus of the respective control area, a coupling constraint is set up for each node. The following active power balances need to be fulfilled:

$$\Delta P_1(k) = P_{e,1}^G(k) - P_{12}(k) - P_{13}(k) - P_{e,1}^H(k) \quad (1.50)$$

$$= f_{P_1}(V_1(k), \theta_1(k), V_2^s(k), \theta_2^s(k), V_3^s(k), \theta_3^s(k)) = 0$$

$$\Delta P_2(k) = P_{e,2}^G(k) + P_{12}(k) - P_{13}(k) - P_{e,2}^H(k) \quad (1.51)$$

$$= f_{P_2}(V_1^s(k), \theta_1^s(k), V_2(k), \theta_2(k), V_3^s(k), \theta_3^s(k)) = 0$$

$$\Delta P_3(k) = P_{e,3}^G(k) + P_{12}(k) + P_{13}(k) - P_{e,3}^H(k) \quad (1.52)$$

$$= f_{P_3}(V_1^s(k), \theta_1^s(k), V_2^s(k), \theta_2^s(k), V_3(k), \theta_3(k)) = 0.$$

Pipeline networks

Implementing the decomposition procedure for natural gas systems, the constraints are arranged in the same way. The constraints $\tilde{\mathbf{g}}_A(\tilde{\mathbf{y}}_A(k)) = 0$, $\tilde{\mathbf{g}}_B(\tilde{\mathbf{y}}_B(k)) = 0$ comprise the volume flow equations of all inner buses as well as the pressure reference settings (slack bus). Coordination is required due to the nodal flow balances at the border buses, since the injected volume flows are dependent on the nodal pressures of the neighboring buses. Inequality constraints consist of pressure limits and compressor limits. No coupling inequality constraints are incorporated. Here, each node serves as border bus as well, thus, a coupling constraint is set up for each node. The

following volume flow balances need to be fulfilled:

$$\Delta F_1(k) = P_{g,1}^G(k) - F_{12}(k) - F_{13}(k) - F_{\text{com},12}(k) - F_{\text{com},13}(k) - P_{g,1}^H(k) \quad (1.53)$$

$$= f_{F_1}(p_1(k), p_2^s(k), p_3^s(k)) = 0$$

$$\Delta F_2(k) = P_{g,2}^G(k) + F_{12}(k) - F_{13}(k) - P_{g,2}^H(k) \quad (1.54)$$

$$= f_{F_2}(p_1^s(k), p_2(k), p_3^s(k)) = 0$$

$$\Delta F_3(k) = F_{12}(k) + F_{13}(k) - P_{g,3}^H(k) \quad (1.55)$$

$$= f_{F_3}(p_1^s(k), p_2^s(k), p_3(k)) = 0,$$

where $F_{\text{com},12}(k)$ and $F_{\text{com},13}(k)$ describe the gas flows into the compressors C_{12} and C_{13} , respectively. For combined electricity and natural gas networks, the constraints are merged. Summarizing, for each controller, there exists one coupling constraint for the electricity and one for the natural gas system.

Resulting objective functions

The resulting objective functions for the controllers are obtained by adding in each case the coupling constraints of the neighboring areas. These constraints are weighted with the corresponding Lagrangian multipliers, obtained by the correspondent neighboring area. For example, the objective of the first controller takes into account the constraints of the second and third controller which are weighted by the Lagrangian multipliers obtained at the previous iteration step. The Lagrangian multipliers related to the electricity system and gas system are referred to as λ_{el} and λ_{gas} , respectively. We then obtain the following objective functions:

$$J_1(\cdot) = \sum_{l=0}^{N-1} q_1^G(k+l)(P_{e,1}^G(k+l))^2 + q_1^N(k+l)(P_{g,1}^G(k+l))^2 \\ + \lambda_{\text{el},23}^s(k) \begin{bmatrix} \Delta P_2(k) \\ \Delta P_3(k) \end{bmatrix} + \lambda_{\text{gas},23}^s(k) \begin{bmatrix} \Delta F_2(k) \\ \Delta F_3(k) \end{bmatrix} \quad (1.56)$$

$$J_2(\cdot) = \sum_{l=0}^{N-1} q_2^G(k+l)(P_{e,2}^G(k+l))^2 + q_2^N(k+l)(P_{g,2}^G(k+l))^2 \\ + \lambda_{\text{el},13}^s(k) \begin{bmatrix} \Delta P_1(k) \\ \Delta P_3(k) \end{bmatrix} + \lambda_{\text{gas},13}^s(k) \begin{bmatrix} \Delta F_1(k) \\ \Delta F_3(k) \end{bmatrix} \quad (1.57)$$

$$J_3(\cdot) = \sum_{l=0}^{N-1} q_3^G(k+l)(P_{e,3}^G(k+l))^2 \\ + \lambda_{\text{el},12}^s(k) \begin{bmatrix} \Delta P_1(k) \\ \Delta P_2(k) \end{bmatrix} + \lambda_{\text{gas},12}^s(k) \begin{bmatrix} \Delta F_1(k) \\ \Delta F_2(k) \end{bmatrix}. \quad (1.58)$$

1.6 Simulation results

Simulations are presented, applying the MPC scheme proposed above to the three-hub system shown in Figure 1.4. Note that the scheme is general according to the discussion above and not only valid or applicable for our illustrative three-hub system. Next the setup of the simulation is given. Then, simulation results in which the centralized and distributed MPC approach are applied are presented. As the considered optimization problems are nonconvex, finding the global optimum cannot be guaranteed when applying numerical methods. However, the values of the centralized problem serve as a reference of optimality and the simulation results obtained by distributed optimization are compared with these values in order to judge the performance of the distributed approach. The solver `fmincon` provided by the Optimization Toolbox of Matlab is used [27].

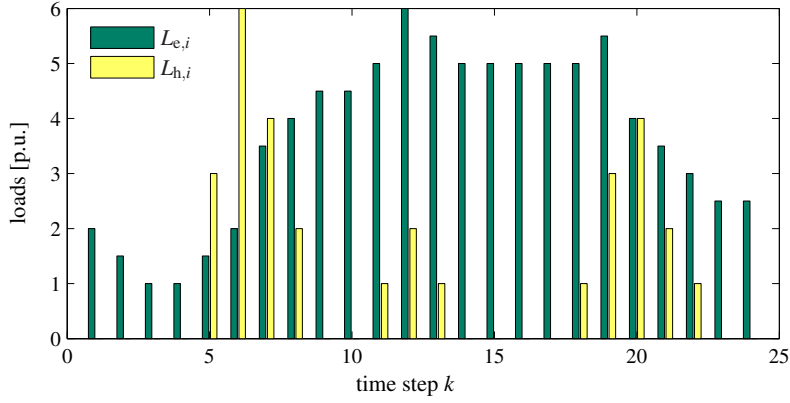
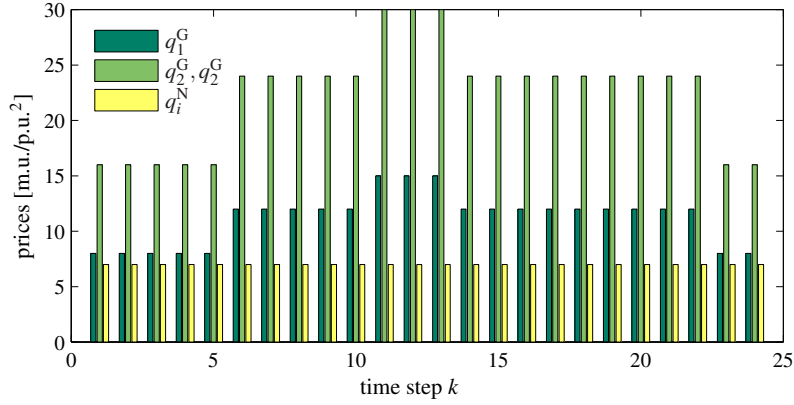
1.6.1 Simulation setup

Each hub has a daily profile of its load demand and the energy prices. Here, we assume that the price and load forecasts are known. However, in reality, there are always forecast errors. As a first study, we assume perfect forecasts and it is believed that the following results are representative also for small forecast errors since the storage devices are able to balance deviations within load forecasts. The given profiles are typical profiles for a household. The electricity and heat loads are assumed to be the same for all hubs and are depicted in Figure 13(a) in per unit (p.u.) values.

Regarding the prices, electricity generation at hubs H_2 and H_3 is twice as expensive as at hub H_1 , as illustrated in Figure 13(b) in m.u./p.u.² values, where m.u. refers to monetary units. The reason for choosing different electricity prices is to obtain three hubs with different setups. (Hub H_1 has a cheap access to electricity and gas, hub H_2 has an expensive electricity and a limited gas access, and hub H_3 has an expensive electricity access and no gas access.) Gas prices remain constant throughout the day.

Regarding the electricity network, bus 1 is modeled as slack bus, i.e., having the voltage angle and voltage magnitude fixed ($V_1(k)$ has a magnitude of 1 p.u. and an angle of 0°). The other two buses are modeled as PV buses, for which the net active power and the voltage magnitude are specified. Also within the gas network bus 1 serves as slack bus, having a fixed pressure value of 1 p.u. The coefficients and simulation parameters used are listed in Table 1.2. Since hub H_2 is assumed to have only access to a network with limited capacity, a flow rate constraint of 2 p.u. is imposed on $P_{g,2}^G(k)$. The gas network is mainly supplied via the large gas network at bus 1, i.e., via $P_{g,1}^G(k)$, which delivers gas to the neighboring buses by means of the two compressors.

Based on the profiles, the total generation costs are minimized for a simulation period of $N_{\text{sim}} = 24$ steps, where one time step corresponds to 1 hour. To analyze the

(a) Electricity $L_{e,i}(k)$ and heat load $L_{h,i}(k)$ profiles.(b) Price profiles for electricity $q_i^G(k)$ and natural gas consumption $q_i^N(k)$.**Fig. 1.13:** Daily profiles used for simulation.**Table 1.2:** Bounds and parameter values for the three-hub system in p.u.

variable	bounds	category	coefficients
V_i	$0.9 \leq V_i \leq 1.1$	μCHP	$\eta_{\text{ge},i}^{\text{CHP}} = 0.3, \eta_{\text{gh},i}^{\text{CHP}} = 0.4$
$P_{e,i}^G$	$0 \leq P_{e,i}^G \leq 10$	F	$\eta_{\text{gh},i}^{\text{F}} = 0.75$
p_i	$0.8 \leq p_i \leq 1.2$	$E_{h,i}^{\text{stb}}$	$E_{h,i}^{\text{stb}} = 0.2$
$p_{\text{inc},i}$	$1.2 \leq p_{\text{inc},i} \leq 1.8$	$e_{h,i}$	$e_{h,i}^+ = e_{h,i}^- = 0.9$
v_i	$0 \leq v_i \leq 1$		
$p_{g,i}^G$	$0 \leq p_{g,1}^G \leq 20, 0 \leq p_{g,2}^G \leq 2$		
E_i	$0.5 \leq E_i \leq 3$		
$M_{h,i}$	$-3 \leq M_{h,i} \leq 3$		

performance of the proposed control scheme, we vary the length of the prediction horizon N used between $N = 1$, i.e., no prediction, and $N = 24$, i.e., predicting for all 24 time steps at once.

1.6.2 Centralized control

First, the results for a specific prediction horizon are analyzed in more detail. Second, the performance of the control scheme operating with different prediction horizon lengths is compared. Finally, the operation costs are presented when comparing the operation of the μ CHP device with and without heat storage support. Furthermore, the costs are compared with the decoupled operation mode, i.e., when the electricity and natural gas system are operated independently of each other, i.e., when no μ CHP devices are in use.

1.6.2.1 Prediction horizon with length $N = 5$

The behavior of the system is illustrated for a prediction horizon with length $N = 5$. This length of prediction horizon is adequate for practical applications as it represents a proper trade-off between control performance on the one side and obtainable forecasts and computational effort on the other side, as is illustrated below in Section 1.6.2.2.

An optimization for 24 time steps is run, at each time step k implementing only the control variables for the current time step k and then starting the procedure again at time step $k + 1$ using updated system measurements. The operational costs for the entire simulation period $[0, 24]$ are $2.73 \cdot 10^4$ m.u. Figure 1.14 shows the evolution of the active power generation and natural gas import at the first hub. The electricity generation mainly corresponds to the electricity load pattern and the natural gas import evolves similar to the heat loads. However, natural gas is also used during time periods, in which no heat is required. During these periods gas is converted by the μ CHP for supporting the electricity generation. The heat produced thereby is stored and used later for the heat supply.

In Figure 1.17, the content of all three storage devices over time is shown for $N = 1, 3, 5, 24$. The dotted line represents the storage behavior for a prediction horizon with length $N = 5$. In general, the storage devices are mainly discharged during the heat load peaks and charged when no heat is required. However, the heat storage devices are not only important for the heat supply but indirectly also for electricity generation, since the μ CHP devices can be operated according to the electricity load requirements by means of the heat storage devices. At high electricity prices, electricity generation via μ CHP is cheaper than via the generators, thus, the μ CHP devices are preferably used for supplying the electricity demand while storing all excessive produced heat. This is also the reason why the storage contents of storages E_1 and E_2 rise again at the end of the simulation. Nevertheless, during the heat

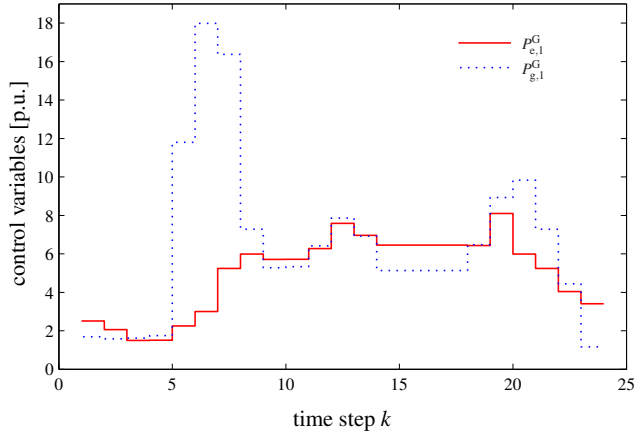


Fig. 1.14: Active power generation $P_{e,1}^G(k)$ and natural gas import $P_{g,1}^G(k)$ of hub H_1 over the simulation horizon.

peak loads all gas is diverted into the furnaces because the thermal efficiencies of the μ CHPs are not sufficient in order to supply the heat loads. During these time periods, the operational costs increase correspondingly.

1.6.2.2 Comparison of different prediction horizon lengths

For showing the effect of prediction, prediction horizons with different lengths N are compared. In order to obtain a fair comparison, the prediction horizon is reduced towards the end of the simulation. Hence, in each case, the controller knows the same data, i.e., the measurements of the same 24 time steps. Figure 1.15 shows the total operation costs defined in (1.36) for different lengths of the prediction horizon N . Generally, the operation costs decrease with increasing prediction horizon. But this is not always the case. Depending on the input profiles, some prediction horizon lengths yield poorer results since the planned actions are suboptimal with respect to the whole simulation horizon. It should be noted that this conclusion is valid for this specific load profiles and that other load profiles might yield other results. As can be seen, a fast decay of the operation costs occurs within prediction horizon lengths $N = 1, \dots, 5$. For longer prediction horizons, not much reduction of the cost is gained, except for optimizing for all 24 time steps at once ($N = 24$). Besides that, computational effort increases with increasing prediction horizon length. Figure 1.16 shows the computation time for different prediction horizon lengths. As can be seen, computational effort increases considerably for prediction horizon lengths larger than $N = 5$.

In Figure 1.17, the storage contents for different lengths of prediction horizons are presented. The horizontal lines indicate the storage limits ($0.5 \leq E_i(k) \leq 3$). At a prediction horizon with a length of $N = 1$ (dotted line) and $N = 3$ (solid line), the

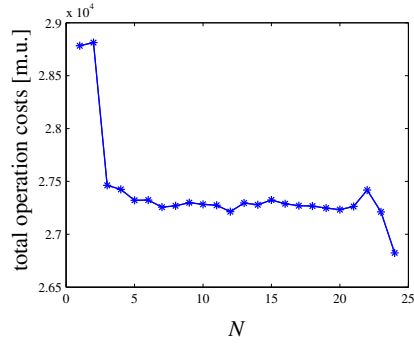


Fig. 1.15: Total operation costs for different lengths of prediction horizon N .

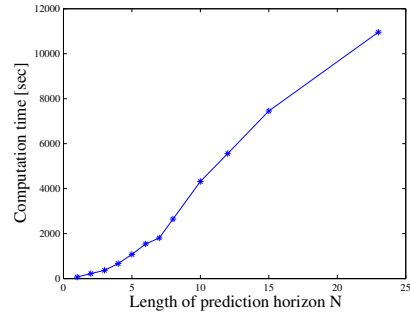


Fig. 1.16: Computation time for different lengths of prediction horizon N .

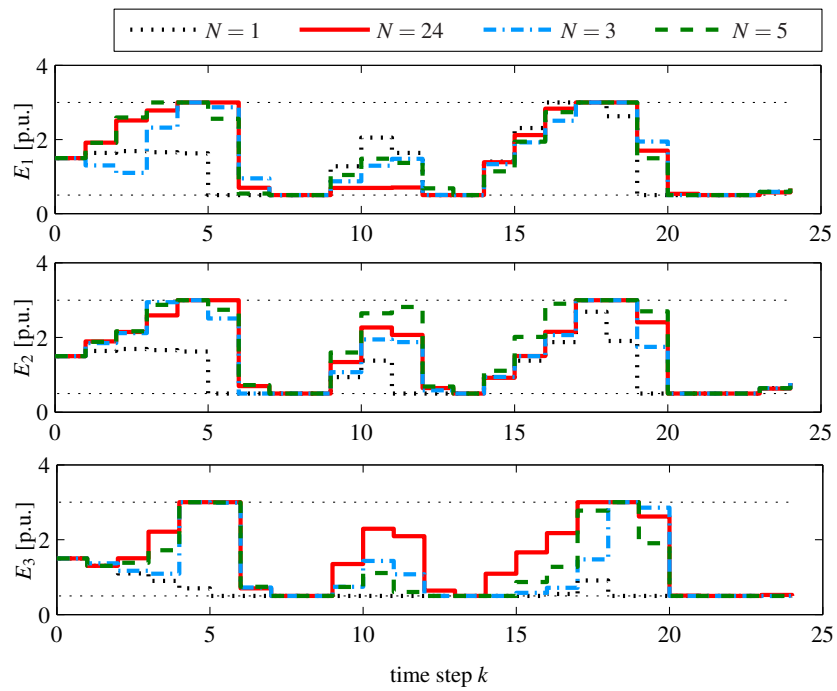


Fig. 1.17: Storage evolution over simulation horizon. Comparison for different lengths of the prediction horizon, $N = 1, 3, 5, 24$.

storage devices are filled up too late or are even emptied (time steps 1–3) because the controller sees the heat load peaks too late. With increasing N , the storage devices are filled up earlier. In fact, the optimization of the system would continuously proceed. For demonstration purposes, the optimization is stopped after 24 time steps. Therefore, no terminal constraint for the storage is imposed, such as requiring the storages to be half full at the end of the simulation period.

When optimizing for all 24 time steps at once the most optimal behavior over the simulation horizon is obtained. The control variables for all next 24 time steps are determined and applied at time step k . But optimizing for all time steps at once is not applicable in practice since the data for the whole next day is normally not known in advance. Moreover, possibly occurring disturbances cannot be handled and computational effort becomes too high. Hence in practice, applying MPC with a properly chosen length of prediction horizon is the best choice. For the application example presented in this paper, a prediction horizon length of $N = 5$ yields the best results. In general, depending on the specifications, a trade-off between control performance and computational effort has to be made. Issues such as obtainable forecasts and size of possible disturbances also influence the choice of an adequate length of prediction horizon.

1.6.2.3 Comparison with decoupled mode

In the following the operation costs are compared for different system setups regarding the μ CHP and the storage devices. The configuration with μ CHP and storage devices serves as base case. In Table 1.3 the increase in costs for the different cases are presented, in each case the optimization is made with a prediction horizon length of $N = 5$. In the first two cases, the μ CHP is utilized and the performance with and without heat storages is compared. Using the μ CHP devices without the heat storages, total operation costs of $2.98 \cdot 10^4$ m.u. are obtained, corresponding to an increase of 9.2%. This is due to the fact that the μ CHP devices cannot be utilized during periods without heat loads because the thereby produced heat cannot be dispensed. The second two cases present the costs obtained in decoupled operation mode, namely when the electricity and natural gas networks are optimized independently of each other. No power is converted by the μ CHP devices in this mode. Running the optimization without μ CHP usage but including the heat storages, to-

Table 1.3: Comparison of operation costs, $N = 5$.

μ CHP	storage	costs [m.u.]	increase
yes	yes	$2.73 \cdot 10^4$	base
yes	no	$2.98 \cdot 10^4$	9.2%
no	yes	$2.94 \cdot 10^4$	7.7%
no	no	$3.07 \cdot 10^4$	12.5%

tal costs of $2.94 \cdot 10^4$ m.u. are obtained. Thus, by decoupling both infrastructures instead of operating them at once, generation costs are increased by 7.7%. Running the simulation with either the μ CHP nor the storage devices yields total costs of $3.07 \cdot 10^4$ m.u., corresponding to an increase of 12.5%. Note that the combination of both devices, μ CHP and storage device, have a higher effect on the total operation costs than each device itself. There exists an interplay between both devices which make both of them necessary.

1.6.3 Distributed control

For the distributed case, again, as a preliminary case study, we assume a perfect forecast, in which no disturbances within the known profiles are occurring. The total generation costs are here minimized for a simulation horizon $N_{\text{sim}} = 10$. The length of the prediction horizon N is chosen as $N = 3$. Hence, an optimization over N time steps is run N_{sim} times, at each time step k implementing only the control variable for the current time step k and then starting a new optimization at time step $k + 1$ with updated system measurements.

The price and load profiles of all hubs used in this study are shown in Figure 1.18. The electricity load $L_{e,i}$ and the gas import prices q_i^N remain constant over time. Variations are assumed only in the prices of the electric energy generation units $q_i^G(k)$ and in the heat load of hub H₂, $L_{h,2}$, in order to exactly retrace the storage behavior. In this study, only two storage devices E₁, E₂ are available for demonstrating the cooperative behavior. Control areas 1 and 2 are supposed to support control area 3 to fulfill its load requirements. Control area 3 has neither a gas access, nor a local heat storage, nor a cheap electricity generation possibility. The other system parameters are as given in Table 1.2.

1.6.3.1 Single simulation step

Feasibility of distributed algorithm

In order to evaluate whether the solution determined by the distributed algorithm is feasible for the real system, the following simulation is run. The quality of the intermediate solutions in case that these would be applied to the system is shown in Figure 1.19. The distributed MPC optimization problem is solved at time step $k = 1$, for $N = 3$. At each iteration counter s , the overall system costs are shown, when applying the control variables determined by the distributed algorithm to the system. The dotted values refer to the infeasible solutions. As the number of iterations increases, the distributed MPC algorithm converges, and, in fact, the solution obtained at the end of the iterations approaches the solution obtained by the centralized MPC approach (200.98 m.u.). After iteration 16, the values of all control variables are feasible. After 39 iterations, the algorithm converges.

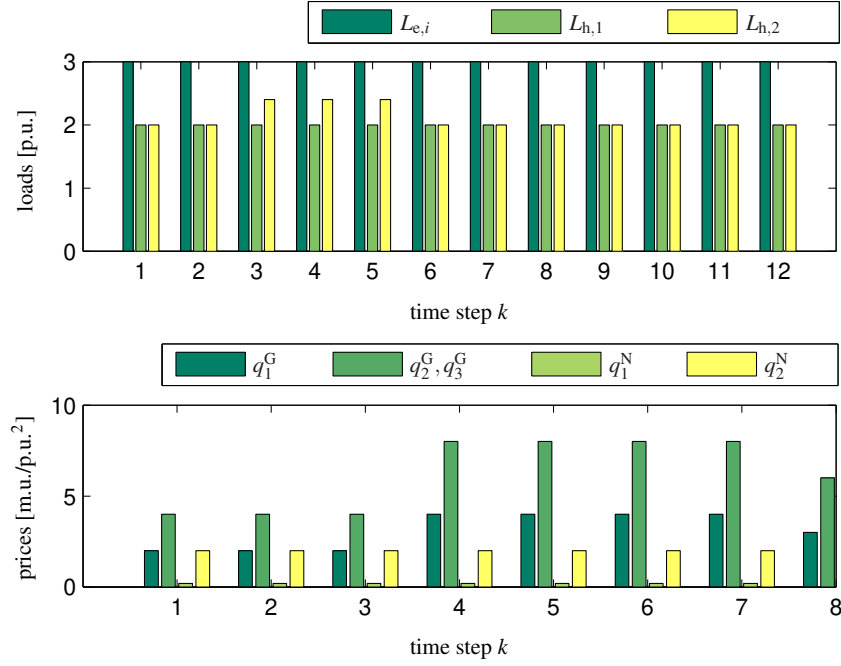


Fig. 1.18: Profile for electricity $L_{e,i}(k)$ and heat loads $L_{h,i}(k)$ (upper plot) and prices for electricity $q_i^G(k)$ and natural gas consumption $q_i^N(k)$ (lower plot).

Basically, the amount of backup energy provided by the storage devices determine whether the solution of the distributed MPC algorithm is feasible. Applying the solution to the system, the control variables are kept fixed, while the values of the storages are varied within their range attempting to fulfill the load requirements, i.e., to find an overall feasible solution. Hence, if the storage devices have not been operated close to their limits at the previous time step, a solution of the distributed algorithm may yield a feasible system solution, although the controller solution is considerably far away from a coordination between the individual control areas.

Convergence between control areas

Running the algorithm for the first simulation step with a prediction horizon length of $N = 3$ yields overall production costs of 200.77 m.u. Figure 20(a) shows the evolution of the objective values of all control areas as well as the total objective value. The costs of area 1 are higher since it contributes the highest amount of energy for overall system. The control variables are plotted in Figure 20(b). Their

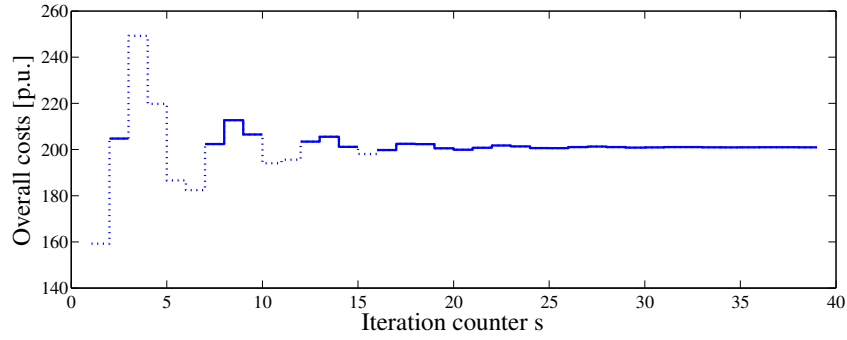


Fig. 1.19: Intermediate solutions of the distributed algorithm applied to the system. Dotted lines represent infeasible solutions, solid lines are feasible solutions.

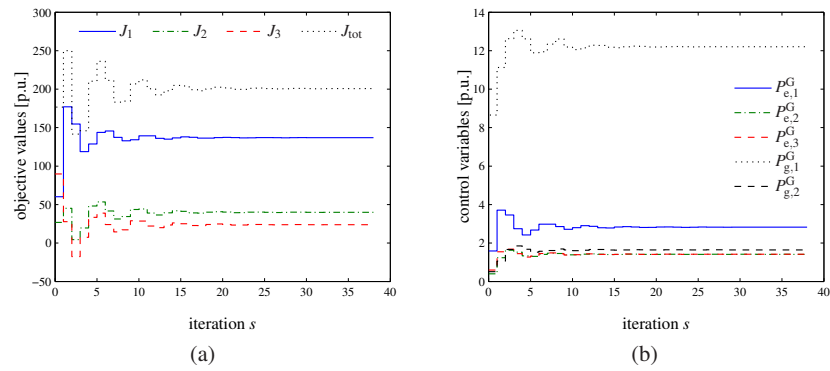


Fig. 1.20: (a) Objective values of areas 1, 2, 3 and total objective value; (b) control variables: active power generation and natural gas import.

steady state values adjust according to the prices for electricity generation and for the natural gas consumption, respectively.

For analyzing convergence between the control areas the evolution of the coupling constraints is plotted. In Figure 1.21, the coupling constraints obtained by the optimization of area 2 are presented. Figure 21(a) shows the active power balances obtained at all node of the electricity system and Figure 21(b) presents the volume flow balances at all nodes of the natural gas system. The active power balance and the volume flow balance as considered by node 2, denoted by $\Delta P_{2,2}$ and $\Delta F_{2,2}$, respectively, remain zero, i.e., the balances are always fulfilled, as they are implemented as hard constraints in the optimization problem of area 2. With increasing iterations, the coupling constraints decrease to zero, i.e., they are fulfilled, indicating that a successful coordination between the control agents has been achieved.

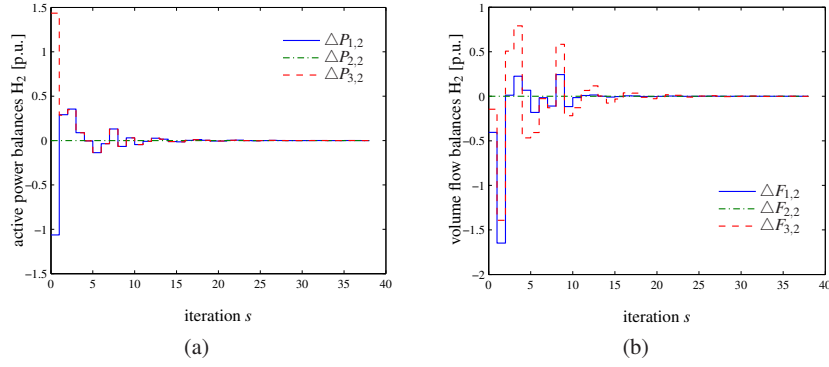


Fig. 1.21: Convergence of coupling constraints at nodes 2: (a) active power balances and (b) volume flow balances.

1.6.3.2 Simulation of multiple time steps

When minimizing the energy costs over the full simulation of N_{sim} time steps, a total cost of 850.62 m.u. is obtained for the load and price profiles given above. Applying centralized MPC, the overall costs are lower, 849.78 m.u., since, due to the imposed convergence tolerance γ_{tol} of the distributed algorithm, the centralized approach finds a slightly different solution at some iteration steps. In Figure 1.22 the active power generation and the natural gas import of hub H_2 are shown. As can be seen, active power generation is reduced at time steps with higher generation costs, i.e., time steps 4–7 and time step 10. During these time steps more gas is consumed. The electrical loads are now predominantly supplied by the μCHP devices in order to save costs. Most of the gas is diverted into the μCHP device and less into the furnace. For still supplying the heat load, the heat storage devices come into operation. Figure 1.23 shows the content of both storage devices evolving over the time steps. Both storage devices start at an initial level of 1.5 p.u. Since the heat load at hub H_2 is increased by 20% at time steps 3–5 (Figure 1.18), storage E_2 attempts to remain full before this increase and then operates at its lower limit during the heat load peaks. At the subsequent electricity price peaks (time steps 6, 7) both storages are recharged. The electrical loads are mainly supplied by the μCHP devices and all excessive heat produced during these time steps is then stored in the storage devices. Storage device E_1 is refilled more than E_2 , as hub H_2 has a limited gas access.

If the controllers have a shorter prediction horizon than $N = 3$, the storage devices are filled up less and also later. With a prediction horizon length of $N = N_{\text{sim}}$, the storage devices are filled up earlier and the lowest costs are obtained, although calculation time becomes considerably longer and the system is insensitive to unknown changes in the load and price profiles.

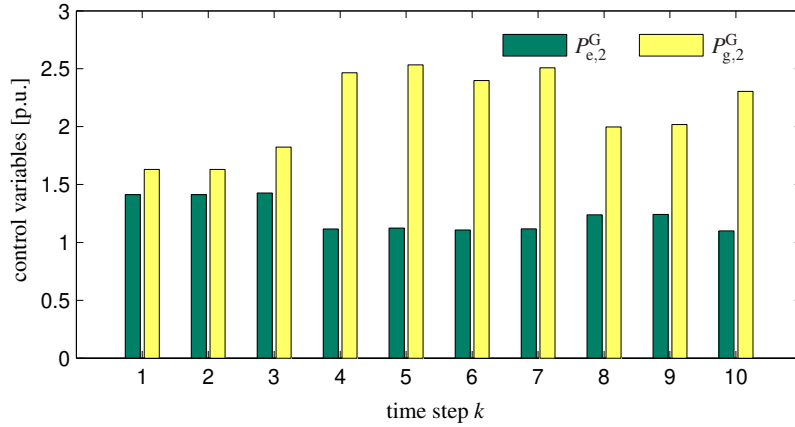


Fig. 1.22: Active power generation $P_{e,2}^G$ and natural gas import $P_{g,2}^G$ of hub H_2 over time.

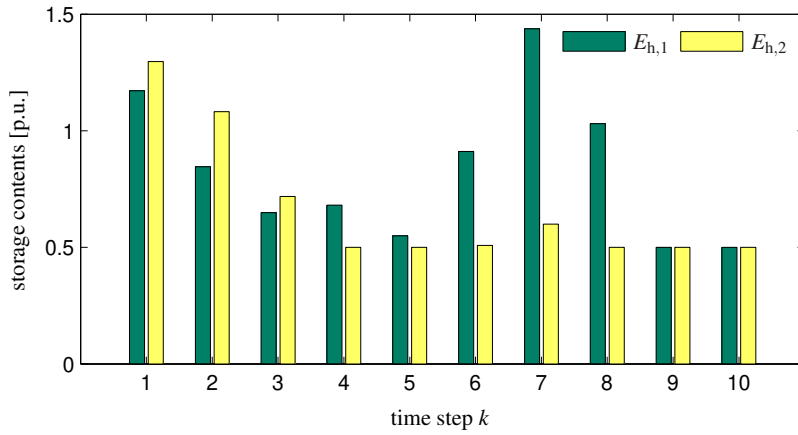


Fig. 1.23: Evolution of storage contents $E_{h,1}$ and $E_{h,2}$ over time.

1.7 Conclusions and future research

In this chapter we have proposed the application of model predictive control to energy hub systems. The dynamics of storage devices, forecasts on energy prices and demand profiles, and operational constraints are taken into account adequately by the predictive control scheme, which is an effective control approach for this type of systems. The performance of different prediction horizons of varying length have been compared. With an increasing length of the prediction horizon the total operation costs decrease, but the computational effort increases accordingly. The analyses show that due to storage capability, even more flexibility on energy conversion in-

side the hubs is provided, which brings about more freedom in system planning and operation.

A distributed model predictive control (MPC) approach has been proposed for solving the overall optimization problem in a distributed way. In a case study, we have analyzed the quality of intermediate solutions obtained throughout the iterations of the proposed approach to ensure that applying the control to the real system yields feasible solutions. A cooperative behavior is shown, where the neighboring areas help to support the system wide objective.

Future research will address the incorporation of forecast errors into the scheme instead of assuming perfect forecasts. The goal is to implement different load forecast models and to analyze what size in forecast error the procedure can handle. Basically, the storage devices are the units that are able to balance a deviation within the load forecasts. Hence, the quality of the forecasts defines the size of the storage. The more appropriate forecasts are available, the smaller storage devices are needed to compensate the load prediction errors.

Furthermore, conditions and measures for guaranteeing convergence have to be investigated more precisely. As the solution spaces of the individual optimization problems are nonconvex, each control agent may have multiple choices for a local minimum. If neighboring agents each go for a local minimum that does not yield a system-wide feasible solution, the agents end up in a situation fighting against each other which results in a hunting or zig-zag behavior. If this zig-zag behavior is not too large in size, the distributed solution still yields a feasible system solution, as the storages can balance out a certain amount of disagreement. In these situations, it has to be decided which one is the dominant area, i.e., which one is decisive in the conflict. This decision is possibly based on economics or other relevant criteria. One aspect of future work will focus on determining which additional information has to be exchanged in order to make the algorithm more robust.

In addition, network operators, which could influence the energy exchanges between the hubs, are to be incorporated to the interconnected hub system. The final goal is to apply the developed procedures to larger systems with more than three hubs. Thereby, multiple hubs probably are taken into the same control area for enabling coordination within reasonable time. Then, firstly coordination *between* the different control areas and then coordination *within* the individual control areas is carried out.

Acknowledgements This research is supported by the project “Vision of Future Energy Networks” (VoFEN) of ABB, Areva T&D, Siemens, and the Swiss Federal Office of Energy, the BSIK project “Next Generation Infrastructures (NGI)”, the Delft Research Center Next Generation Infrastructures, the European STREP project “Hierarchical and distributed model predictive control (HD-MPC)”, and the project “Multi-Agent Control of Large-Scale Hybrid Systems” (DWV.6188) of the Dutch Technology Foundation STW.

References

- [1] A. Alessio and A. Bemporad. Decentralized model predictive control of constrained linear systems. In *Proceedings of the European Control Conference 2007*, pages 2813–2818, Kos, Greece, July 2007.
- [2] S. An, Q. Li, and T. W. Gedra. Natural gas and electricity optimal power flow. In *Proceedings of the 2003 IEEE PES Transmission and Distribution Conference*, pages 138–143, Dallas, Texas, September 2003.
- [3] M. Arnold, R. R. Negenborn, G. Andersson, and B. De Schutter. Distributed control applied to combined electricity and natural gas infrastructures. In *Proceedings of the International Conference on Infrastructure Systems*, Rotterdam, The Netherlands, November 2008.
- [4] D. P. Bertsekas. *Nonlinear Programming*. Athena Scientific, Belmont, Massachusetts, 2003.
- [5] I. Bouwmans and K. Hemmes. Optimising energy systems: Hydrogen and distributed generation. In *Proceedings of the 2nd International Symposium on Distributed Generation: Power System Market Aspects*, pages 1–7, Stockholm, Sweden, October 2002.
- [6] E. F. Camacho and C. Bordons. *Model Predictive Control*. Springer-Verlag, New York, New York, 2004.
- [7] G. Chicco and P. Mancarella. A comprehensive approach to the characterization of trigeneration systems. In *Proceedings of the 6th World Energy System Conference*, Turin, Italy, July 2006.
- [8] A. J. Conejo, F. J. Nogales, and F. J. Prieto. A decomposition procedure based on approximate newton directions. *Mathematical Programming, Series A*, 93(3):495–515, December 2002.
- [9] M. Geidl and G. Andersson. Optimal coupling of energy infrastructures. In *Proceedings of PowerTech 2007*, pages 1398–1403, Lausanne, Switzerland, July 2007.
- [10] M. Geidl and G. Andersson. Optimal power flow of multiple energy carriers. *IEEE Transactions on Power Systems*, 22(1):145–155, 2007.
- [11] H. M. Groscurth, T. Bruckner, and R. Kümmel. Modeling of energy services supply systems. *Energy*, 20(9):941–958, January 1995.
- [12] A. Hajimiragha, C. Canizares, M. Fowler, M. Geider, and G. Andersson. Optimal energy flow of integrated energy systems with hydrogen economy considerations, August 2007. Presented at the IREP Symposium Bulk Power System Dynamics and Control – VII.
- [13] J. Hernandez-Santoyo and A. Sanchez-Cifuentes. Trigeneration: An alternative for energy savings. *Applied Energy*, 76(1–3):219–277, 2003.
- [14] B. H. Kim and R. Baldick. Coarse-grained distributed optimal power flow. *IEEE Transactions on Power Systems*, 12(2):932–939, May 1997.
- [15] B. H. Kim and R. Baldick. A comparison of distributed optimal power flow algorithms. *IEEE Transactions on Power Systems*, 15(2):599–604, May 2000.

- [16] G. Koepfel and G. Andersson. The influence of combined power, gas and thermal networks on the reliability of supply. In *Proceedings of 6th World Energy System Conference*, pages 646–651, Turin, Italy, July 2006.
- [17] P. Kundur. *Power System Stability and Control*. McGraw-Hill, New York, New York, 1994.
- [18] R. H. Lasseter and P. Piagi. Microgrid: A conceptual solution. In *Proceedings of the IEEE 35th Annual Power Electronics Specialists Conference*, pages 4285–4290, Aachen, Germany, June 2004.
- [19] J. M. Maciejowski. *Predictive Control with Constraints*. Prentice Hall, Harlow, England, 2002.
- [20] E. S. Menon. *Gas Pipeline Hydraulics*. Taylor & Francis, New York, New York, 2005.
- [21] M. S. Morais and J. W. Marangon Lima. Natural gas network pricing and its influence on electricity and gas markets. In *Proceedings of the 2003 IEEE Bologna PowerTech Conference*, Bologna, Italy, June 2003.
- [22] R. R. Negenborn, B. De Schutter, and J. Hellendoorn. Multi-agent model predictive control for transportation networks: Serial versus parallel schemes. *Engineering Applications of Artificial Intelligence*, 21(3):353–366, April 2008.
- [23] A. J. Nogales, F. J. Prieto, and A. J. Conejo. A decomposition methodology applied to the multi-area optimal power flow problem. *Annals of Operations Research*, 120(1-4):99–116, April 2003.
- [24] F. J. Nogales, F. J. Prieto, and A. J. Conejo. A decomposition methodology applied to the multi-area optimal power flow problem. *Annals of Operations Research*, 120:99–116, April 2003.
- [25] R. Scattolini. Architectures for distributed and hierarchical model predictive control – A review. *Journal of Process Control*, 19(5):723–731, May 2009.
- [26] M. Shahidehpour, Y. Fu, and T. Wiedman. Impact of natural gas infrastructure on electric power systems. *Proceedings of the IEEE*, 93(5):1024–1056, 2005.
- [27] The Mathworks. *Optimization Toolbox User’s Guide*, 2008.
- [28] A. N. Venkat, J. B. Rawlings, and S. J. Wright. Stability and optimality of distributed model predictive control. In *Proceedings of 44th IEEE Conference on Decision and Control*, pages 6680–6685, Seville, Spain, December 2005.